eNeuro

Research Article: Confirmation | Development

Postnatal Increases in Axonal Conduction Velocity of an Identified *Drosophila* Interneuron Require Fast Sodium, L-Type Calcium and Shaker Potassium Channels

https://doi.org/10.1523/ENEURO.0181-19.2019

Cite as: eNeuro 2019; 10.1523/ENEURO.0181-19.2019

Received: 15 May 2019
Revised: 6 June 2019
Accepted: 12 June 2019

Title: Postnatal Increases in Axonal Conduction Velocity of an Identified *Drosophila* Interneuron Require Fast Sodium, L-Type Calcium and Shaker Potassium Channels

Abreviated title: Postnatal increase of axonal conduction velocity

Dimitrios Kadas [1], Carsten Duch [2], Christos Consoulas [1]

1 Laboratory of Experimental Physiology, National and Kapodistrian University of Athens, 11527 Athens, Greece
2 Institute of Developmental Biology and Neurobiology, Johannes Gutenberg University Mainz, 55122 Mainz, Germany

Corresponding author
Dimitrios Kadas (PhD)
Laboratory of Experimental Physiology
Medical School,
National and Kapodistrian University of Athens
Micras Asias 75, Goudi,
GR-11527, Athens
GREECE
tel. : +30-210-746-2701
FAX : +30-210-746-2571
e-mail: dimkadas@gmail.com

Number of pages: 46
Number of figures (8), tables (2),
Number of words for Abstract (246), Introduction (480), and Discussion (1750)
Conflict of Interest: No conflict of interest
Acknowledgements: DK was funded by the Hellenic Ministry of Education, Research and Religion within the framework of the action “SUPPORT OF POSTDOCTORAL RESEARCHERS” of the OP “Development of Human Resources, Education and Lifelong Learning ", 2014-2020, which is being implemented by the IKY and was co-financed from the European Social Fund and the Greek Public. Support by the German Research Foundation (DFG, DU 331/6-2) to CD is gratefully acknowledged.

E-mail address of all Authors
Duch Carsten: cduch@uni-mainz.de
Consoulas Christos: cconsoul@med.uoa.gr

Keywords: giant fiber, *Drosophila*, postnatal, action potential propagation, voltage gated ion channels

Abstract

During early postnatal life, speed up of signal propagation through many central and peripheral neurons has been associated with an increase in axon diameter or/and myelination. Especially in unmyelinated axons postnatal adjustments of axonal membrane conductances is potentially a third mechanism but solid evidence is lacking. Here we show that axonal action potential conduction velocity in the *Drosophila* giant fiber interneuron (GF), that is required for fast long distance signal conduction through the escape circuit, is increased by 80% during the first day of adult life. Genetic manipulations indicate that this postnatal increase in action potential conduction velocity in the unmyelinated GF axon is likely owed to adjustments of ion channel expression or properties rather than axon diameter increases. Specifically, targeted RNAi knockdown of either Para fast voltage-gated sodium, Shaker potassium (*Kv1* homologue), or surprisingly, L-type like calcium channels counteracts postnatal increases in GF axonal conduction velocity. By contrast, the calcium-dependent potassium channel Slowpoke (BK) is not essential for postnatal speeding, though it also significantly increases conduction velocity. Therefore, we identified multiple ion channels that function to support fast axonal action potential conduction velocity, but only a subset of these are regulated during early postnatal life to maximize conduction velocity. Despite its large diameter (~ 7µm) and postnatal regulation of multiple ionic conductances, mature GF axonal conduction velocity is still 20-60 times slower than that of vertebrate Aβ sensory axons and α motoneurons, thus

unraveling the limits of long range information transfer speed through invertebrate circuits.

Significance statement

An effective mechanism to increase information processing speed through neural circuits is enhancing plasma membrane insulation through optimizing myelination, a means that cannot be capitalized on un-myelinated invertebrate axons. We identify postnatal adjustments of the expression levels of fast sodium, Shaker potassium, and L-type calcium channels as a mechanism to almost double axonal conduction velocity in the *Drosophila* giant fiber axon, the core component for long range information transfer through a neural circuit optimized for fast escape responses. However, despite the regulation of multiple ion channels, mature giant fiber axonal conduction velocity still lacks magnitudes of order behind that of myelinated vertebrate fibers, thus hinting to long distance information transfer as a size-constrain in the evolution of invertebrate circuits.

INTRODUCTION (480 words)

Central nervous system development is not completed at birth, but early postnatal life is accompanied by structural and physiological refinement of neuronal circuits to adjust function to the new life conditions (Webb et al., 2001). In mammals, the first 2-3 weeks after birth are characterized by changes in synapse number (Kano et al., 2018) and strength (Maffei, Turrigiano, 2008) as well as changes in passive and active membrane properties to adjust network activity (Fulton, 1986; Viana et al., 1994; Zou, Hablitz, 1996; Vincent, Tell, 1997; Cabanes et al., 2002).

Moreover, in many central and sensory neurons axonal action potential (AP) conduction velocity is increased postnatally, thus accelerating the speed of long rang information transfer through the nervous system (NS). Mis-regulation of this mechanism has been linked to neurological and psychiatric disorders, such as epilepsy and schizophrenia (Scharfman, McCloskey, 2009; Jaaro-Peled et al., 2009; Duncan et al., 2010; Pun et al., 2012). In the vertebrate NS axonal conduction velocity is most effectively increased by myelination (Peters and Muir, 1959; Gibson et al., 2014) and this process extends far into postnatal life (Barnea-Goraly, 2005). In unmyelinated axons, conduction velocity can potentially be regulated by changes in diameter, but up-regulation is limited by space constraints. As an additional mechanism, changes in axonal ionic conductances have been suggested (Foster et al., 1982; Fitzgerald, 1985, 1987;

Fulton, 1987). Although the spatial and temporal patterns of ion channel expression are regulated differentially during NS postnatal development, the contributions of these processes to adjustments of axonal conduction velocity are incompletely understood.

We employ a combination of *Drosophila* genetics and electrophysiology to unravel ionic mechanisms that cause postnatal increases in AP propagation speed in an identified interneuron of the Giant Fiber System (GFS). The GFS is an anatomically and electrophysiologically well characterized neural circuit which mediates the jump-and-flight escape reflex in response to a threatening stimulus. The large diameter giant fiber (GF) interneuron receives sensory input in the brain and relays this information via a descending axon to the escape motor circuit in the ventral nerve cord (King, Wyman, 1980; Tanouye, Wyman, 1980; Trimarchi, Schneiderman, 1993; Hammond, O'Shea, 2007). Therefore, axonal conduction velocity through the GF axon is critical for fast escape.

We demonstrate that postnatal adjustments of ion channel expression in the GF interneuron increase axonal conduction velocity by 80% during the first day of adult life. Our data indicate that increases in the expression of fast voltage-gated sodium, Shaker potassium (*Kv1* homologue), and to our surprise, L-type like calcium channels mediate postnatal increases in GF axonal conduction velocity. Moreover, other active conductances, such as the BK channel, Slowpoke, also increase conduction velocity, but they do not substantially affect postnatal speeding. Therefore, we identified multiple ion channels that function to support fast axonal action potential conduction velocity, but only a subset of these are

regulated during postnatal life to tune the unmyelinated GF axon to maximum speed.

MATERIALS AND METHODS

Drosophila strains and culture. Flies were raised on standard corn flour-yeast-agar medium at 24ºC in a humidified incubator. Adult 1 hour post-eclosion and 24 hours post-eclosion flies of both sexes were used for all experiments. The *GF-split-Gal4* strain [*17A04_p65ADZp (attp40); 68A06_ZpGdbd (attP2)*], which drives expression in the two giant fiber interneurons only (von Reyn et al., 2014), was crossed to the following strains containing UAS insertions: y^1 v^1*; P{UAS-GFP.VALIUM10}attP2* used as a control (Bloomington Stock Center, 35786; RRID:BDSC_35786), y^1 sc^* v^1*; P{TRiP.HMS00868}attP2* that expresses dsRNA for RNAi of *para* (Bloomington Stock Center, 33923; RRID:BDSC_33923), y^1 sc^* v^1*; P{TRiP.HMS00294}attP2* that expresses dsRNA for RNAi of *DmCa1D* (Bloomington Stock Center, 33413; RRID:BDSC_33413), y^1 sc^* v^1*; P{TRiP.HMC03576}attP40* that expresses dsRNA for RNAi of *shaker* (Bloomington Stock Center, 53347; RRID:BDSC_53347), y^1 sc^* v^1*; P{TRiP.HMS05837}attP40* that expresses dsRNA for RNAi of *shal* (Bloomington Stock Center, 67976; RRID:BDSC_67976), y^1 sc^* v^1*; P{TRiP.HMC04093}attP40* that expresses dsRNA for RNAi of *slowpoke* (Bloomington Stock Center, 55405; RRID:BDSC_55405), y^1 w^**; PUAS-NaChBac-EGFP}1/TM3,* Sb^1 that expresses EGFP-tagged bacterial sodium channel (NaChBac) (Bloomington Stock Center, 9467; RRID:BDSC_9467). For light microscopic analysis of Shaker channels along the GF axon, a protein trap fly strain (Bloomington Stock Center, 59423; RRID:BDCS_59423) with endogenously GFP-tagged Shaker channels (y^1w^*

181 Mi{PT-GFSTF.2}Sh$^{MI10885\text{-}GFSTF.2}$) was recombined with the GF-split-Gal4 line and
182 UAS-cd4-tomato (w;GMR17A04-pBPp65ADZpUw attP40 UAS-cd4::td-
183 tomato;GMR68A06-pBPZpGAL4DBDUw attP2). The homozygous recombinant
184 expresses GFP tagged shaker channels and UAS-cd4-tomato in the GF.
185
186 *Effectiveness of RNAi constructs used*
187 Although we have not measured the RNAi knock down efficacy in the giant fiber
188 interneuron, four out of the five UAS-RNAi constructs used in this study have
189 previously been validated in *Drosophila* motoneurons. The RNAi for DmCa1D
190 calcium channels (Bloomington Stock Center, 33413; RRID:BDSC_33413)
191 causes a 70% reduction on larval motoneuron L-type calcium current as
192 measured by somatic voltage clamp recordings (Kadas et al., 2017). This has
193 further been confirmed by immunocytochemistry for Dmca1D in larval
194 motoneuron somata (Kadas et al., 2017) and by calcium imaging (Schützler et
195 al., 2019). UAS-slo-RNAi (Bloomington Stock Center, 55405;
196 RRID:BDSC_55405) has been tested in with the same Gal4 driver in the same
197 types of larval motoneurons and causes a reduction in slow mediated transient
198 outward current by about 50% (Kadas et al., 2015). Therefore, we expect knock
199 down efficacy of slo-RNAi in the GF to be slightly lower than that of Dmca1D-
200 RNAi. The UAS-Shal RNAi construct has been validated to cause more than
201 80% of shal mediated outward current by electrophysiological studies in the
202 same larval motoneurons (Schaefer et al., 2010), and knock down efficacy has
203 been further confirmed in adult *Drosophila* motoneurons (Ryglewski, Duch,

204 2009). For UAS-para-RNAi knock-down efficacy has not been quantified in
205 *Drosophila* neurons. However, effectiveness and specificity have been validated
206 indirectly by showing that UAS-para-RNAi has similar effects like para
207 hypomorphic mutations (Kaas et al., 2016).
208
209 *Electrophysiological preparation and recordings*. Flies were anesthetized briefly
210 glued to a thin metal wire attached to the neck with cyanoacrylate adhesive
211 allowed to recover from anesthesia at least for 30 min. To stimulate electrically
212 the GF neurons or thoracic motoneurons, a pair of uninsulated tungsten
213 electrodes was used to penetrate the eyes or thorax, respectively. A similar
214 electrode was used to record from the DLM5-6 or TTM. A fourth tungsten
215 reference electrode was placed into the scutellum or the abdomen (Kadas et al.,
216 2012).
217 Brain stimulation was performed by delivering stimuli (0.15ms in duration) with a
218 Grass S88 stimulator (W. Warwick, RI U.S.A.), while DLM or TTM muscle action
219 potentials were acquired in the 300Hz to 10KHz frequency range and amplified
220 100X by a differential AC amplifier (A-M systems model 1700). Data were
221 digitized with an analogue-to-digital converter (Digidata 1200, Molecular Devices)
222 and without filtering were analyzed and displayed with Clampex 8.1 version
223 software (Molecular Devices).
224
225 *Confocal microscopy.* All images were acquired with a Leica SP8 confocal laser
226 scanning microscope. (Leica Microsystems Inc, RRID:SSR_004098) with

excitation wavelengths at 488 nm (Argon laser) and at 561 nm (DPSS laser). Detection was conducted with photomultipliers at wavelengths between 495 and 515 and between 570 and 600 nm, respectively. Giant fiber diameter was measured live in freshly dissected animals with a 63x water dipping lense and a z-step size of 1 µm. Co-localization analysis of GFP-tagged shaker channels and the GF interneuron was conducted in fixed and cleared preparations using a 40x oil lens (NA: 1.25). Maximum magnification used was zoom factor 3.5, and 290 nm z-step distances, thus yielding voxel dimensions of 86 x 86 x 290 nm (x,y,z).

Statistical analysis. Statistics were performed with GraphPad Prism 6.00 for Windows (La Jolla California USA, www.graphpad.com). Data were tested for normality (D'Agostino & Pearson omnibus normality test) and unpaired t-test was used to compare between pairs. Data were presented as means and SEM, and significance levels were defined as *$p < 0.05$; ** $p < 0.01$, ***$p < 0.001$ and **** $p<0.0001$.

RESULTS

GF conduction velocity increases over the first day of adult life

On each side of the *Drosophila* CNS the giant fiber system (GFS) consists of a Giant Fiber (GF) interneuron that receives sensory information to its dendrites located in the brain and relays this information through a descending axon to two thoracic motor sub-circuits: the GF-TTM (tergotrochanteral muscle) system, controlling the extension of mesothoracic legs during escape jumping, and the GF-DLMs (dorsal longitudinal flight muscles) system, controlling wing downstroke during flight initiation (Fig. 1A). In the GF-TTM and GF-DLM pathways, the GF makes mixed electrical and chemical (cholinergic) synapses with the TTM jumping motoneuron (TTMn) and the peripherally synapsing interneuron (PSI) (Sun, Wyman, 1996; Allen et al., 1999; Blagburn et al., 1999; Phelan et al., 1996; Allen, Murphey, 2007). The PSI synapses directly onto the axons of the five motoneurons (MN1-5) that innervate the dorsal longitudinal flight muscles (DLMs). MN1-4 innervate the ventralmost 4 DLM fibers, whereas MN5 innervates the two dorsalmost DLM fibers (Fig. 1A; King, Wyman, 1980; Koto et al., 1981; Ikeda, Koenig, 1988; Sun, Wyman, 1997; Koenig, Ikeda, 2005; Allen et al., 2006). The GF to DLM flight muscle pathway comprises one synapse (PSI to MN1-5) more than the GF to TTM pathway (Fig. 1A), thus adding the time for one chemical synaptic transmission onto the signal delay between GF and muscle. Therefore, the typical escape response is a jump followed by flight.

To investigate whether the GF interneuron and /or the downstream motor circuits are subject to functional changes during early postnatal life, circuit performance was compared by electrophysiological recordings in newly eclosed (1hour Post-Eclosion, 1hPE) and 1 day old mature flies (24 hours Post-Eclosion, 24hPE). We bypassed all sensory neurons and synaptic input computation times in the GF dendrites by direct electrical stimulation of the GF interneuron. Electrical stimulation of the GF elicits a muscle potential in the TTM and in the DLM 5-6 muscles (fig. 1Ai, ii). The response latency (the time between GF stimulation and muscle potential; fig. 1B) is the sum of the durations for action potential conduction through the GF, PSI and respective motoneuron axons, plus the time for synaptic transmission. As stated above, for the DLM branch, the PSI to MN5 synaptic delay adds to this latency (Tanouye, Wyman, 1980; Engel, Wu, 1992; Kadas et al., 2012). Therefore the latency of the GF-DLM5-6 (1.45 ± 0.03ms) pathway is significantly (statistical test and p values are provided in figure legends) longer than that of the GF-TTM (1.13 ± 0.02ms) pathway (fig. 1Aii, 1Bi, 1Biii, 1Ci), although the net effect size is only about 0.3 ms, indicating that fast chemical synaptic transmission between PSI and MN5 takes only about one third of a millisecond. Please note that synaptic transmission between the GF and the TTMn is dominated by the electrical component of the mixed synapse. If the electrical component is blocked, the chemical component of the GF/TTMn synapse increases the latency in the GF-TTM pathway almost to the level of the GF-DLM5-6 pathway (Allen, Murphey, 2007; Pézier et al., 2016).

Comparing the response latency of the GF-DLM5-6 branch between one hour and one day old flies reveals a significant shortening during the first day of postnatal life from 1.66 ± 0.02ms at 1hPE to 1.45 ± 0.03ms at 24hPE (fig. 1Ai, 1Aii, 1Bi, 1Ci). Similarly, 1 day old flies exhibit a shorter GF-TTM latency response (1.13 ± 0.02ms) in comparison to 1 hour old flies (1.32 ± 0.02ms; fig.1Ai, 1Aii, 1Biii, 1Ci). Therefore, during the first day of adult life (1-24hPE), response latency of both branches of the GFS is decreased by ~0.2 ms, which equals to an improvement of 14% for the GF-DLM branch (0.21ms) and 17% for the GF-TTM branch (0.19ms; fig. 1Bi, 1Biii, 1Ci). Additional measurements at 48 hrs post eclosion indicated that postnatal maturation was completed by 24 hrs because response latency did not further decrease at 48 hrs (figs. 1Ciii, Civ). Measurements at 12 hrs revealed intermediated values as compared to 1 hr and 24 hrs post eclosion (figs. 1Ciii, Civ)., thus indicating that conduction velocity is likely steadily increased during the first day of adult life. Although net effect size is only ~0.2 ms, this increase in conduction velocity may be of biological relevance considering that it is close to the normal difference of information processing speed through the GF-TTM versus the GF-DLM path, which ensures that jumping precedes flight initiation (see above). A similar net decrease in latency in both GFS branches seems important to maintain the time difference in jump and succeeding flight initiation, and it indicates functional maturation of common circuit elements (axons/synapses). We next aimed at pinpointing the cellular site that underlies the postnatal increases in information transfer.

To test for potential maturation of the motoneurons and/or the neuromuscular synapses, we stimulated the motoneurons directly by inserting tungsten electrodes into the thoracic nerve cord and recorded the responses from the DLM and the TTM muscle, respectively. The latency between motoneuron activation and muscles responses of 1 hour old flies was not significantly different from that of 1 day old flies, for both, the DLM branch (1hPE 0.95 ± 0.03ms, 24hPE 0.97 ± 0.03ms; fig. 1A, 1Bii, 1Cii) and the TTM branch (1hPE 0.80± 0.04ms, 24hPE 0.84 ± 0.02ms; fig. 1A, 1Biv, 1Cii). Hence, motoneuron axonal conduction speed and neuromuscular transmission delay do not undergo postnatal changes. This leaves GF axonal conduction speed as cause for postnatal speeding of GF.

The action potential conduction time in the GF axon can be estimated by subtracting the TTMn-to-TTM latency from the GF-to-TTM latency. Note that the GF to TTMn synapse is dominated by electrical transmission, and thus, does not add notable time to the latency. According to this calculation the GF axonal conduction duration decreased by 80% during the first day of postnatal period, from 0.52 ± 0.04ms in 1hPE flies to 0.29 ± 0.03ms in 24hPE flies (~0.23ms; fig. 1A, 1Ciii, table1). Considering that the axon of the GF is approximately 0.6mm long, this equals to an increase in axonal conduction velocity from 1.15 ± 0.09m/s at 1hPE to 2.07 ± 0.21m/s in 24PE flies (fig. 1A, 1Civ, table 2). We next aimed at addressing the ionic basis of this postnatal increase in axonal conduction velocity of the GF interneuron.

340

341 **Voltage-gated sodium and L-type calcium channels contribute to the GF**
342 **conduction velocity increase postnatally**

343

344 Potential mechanisms underlying postnatal increases in axonal conduction
345 velocity are (i) an enlargement in axon diameter (this would result in decreased
346 axial resistance, thus increasing the length constant λ; Hodgkin, 1954), (ii)
347 improving glial wrapping (this would result in increased membrane resistance,
348 thus increasing λ; Moore et al., 1978), and (iii) hypothetically, changes in the
349 complement, properties, and/or densities of ion channels located in the axonal
350 membrane. First, axon diameter changes can be ruled unlikely because it has
351 been suggested that the axon of the GF reaches its final diameter before
352 eclosion (Allen et al., 1998). Indeed, confocal images demonstrate that the GF
353 outer axon diameter (~7µm) is not different between 1hPE and 24hPE flies (fig.
354 2). But note that CLSM just uncovers the outer axon diameter. EM would be
355 required to rule out small changes in the effective inner diameter that determines
356 axoplasmatic resistance. However, we feel that subtle differences in effective
357 axon diameter that might be hidden to CLSM diameter measurements are
358 difficult to reconcile with the observed 80% increase in conduction velocity.
359 Second, the GF is a non-myelinated invertebrate axon, thus making major effects
360 of glial insulation on action potential conduction speed unlikely. Please note that
361 GF axonal conduction velocity is roughly similar to that of unmyelinated C fibers
362 in vertebrates (see discussion). Therefore, we hypothesized that postnatal

changes in the expression of axonally localized voltage-gated ion channels may underlie postnatal AP conduction velocity increases in the GF.

To test this, we manipulated the expression levels of selected ion channels specifically in the GF by targeting UAS-transgenes with a *split-GAL4* driver that expresses solely in the GF interneurons (von Reyn et al., 2014), and compared axonal conduction velocity at 1h (1hPE) and at 24 post adult eclosion (24hPE). This approach ideally requires identical levels of RNAi knock down efficacy in the GF interneuron at both stages. To exclude largely different expression levels of Gal4 at both staged, we estimated knock-down efficacy in the GF by expressing UAS-RNAi for GFP under the control of the GF selective *split-GAL4;UAS-mcd8-GFP* driver and compared fluorescence intensity at both stages (figs. 2D-G). At 1hPE targeted expression of UAS-GFP-RNAi decreased mean GFP fluorescence intensity in the GF interneuron highly significantly (figs. 2D, F) by ~70% (fig. 2G), thus demonstrating significant effects of RNAi at 1hPE. GFP fluorescence was not further decreased at 24hPE (figs. 2D, F, G). Although this approach provides only a rough estimate of RNAi knock down efficacy, and generalization for different RNAi constructs is not readily possible, these data indicate that UAS-RNAi expression in the GF may provide roughly similar knock-down efficacy at 1h and at 24hPE. However, this does not exclude different knock down efficacies of UAS-RNAi constructs for different ion channels. Four of the five UAS-RNAi constructs for different ion channels used in this study (see below) have previously been confirmed to cause 50-70% knock-down efficacy in larval *Drosophila* motoneurons by means of electrophysiology and/or

386 immunocytochemistry (see methods). Taken together, it seems plausible to
387 assume that each RNAi constructs used caused knock down of the respective
388 channels in the GF neuron, and that for a given ion channel knock down efficacy
389 was similar at both stages tested.

390 We first tested the contribution of voltage-gated sodium channels for
391 axonal conduction velocity. Fast sodium channels are required for action
392 potential generation and propagation in the GF (Tanouye, Ferrus, 1985; Tanouye
393 et al., 1981; von Reyn et al., 2014). The only gene encoding fast voltage-gated
394 sodium channels in *Drosophila* is *paralytic* (*para)* or $DmNa_v$ (Feng et al., 1995;
395 Mee et al., 2004). We lowered the amount of *para* expression in the GF
396 interneuron by targeted expression of *para*-RNAi. For both stages tested (1hPE
397 and 24hPE), this resulted in a significant decrease in axonal conduction velocity
398 in the GF interneuron (figs. 3A, B), which was calculated from measurements of
399 the response latency increases in the GF-TTM pathway with and without para
400 RNAi (figs. 3Bi, 3Biii, 3Ci). The latency between TTMn and TTM was not affected
401 because the RNAi knockdown was targeted to the GF only (figs. 3Bii, 3Biv, 3Cii).
402 Keeping in mind that the GF axonal conduction time equals the time difference
403 between the GF-TTM and the TTMn-TTM latencies, *para* RNAi knockdown in the
404 GF increases axonal conduction time from 0.52 ± 0.04ms to 0.69 ± 0.04ms at
405 1hPE and from 0.29 ± 0.03ms to 0.47 ± 0.03ms at 24hPE (fig. 3Ciii, table1). This
406 corresponds to a 32% decrease in GF axonal conduction velocity at 1hPE (1.15
407 ± 0.09m/s in control to 0.87 ± 0.05m/s in *para* RNAi knockdown), but in a 62%
408 decrease in conduction velocity at 24hPE (from 2.07 ± 0.21m/s in control to 1.28

409 ± 0.08m/s in *para* RNAi knockdown) (fig. 3A, 3Civ, table2). Therefore, *para* RNAi
410 had a stronger effect in more mature GF interneurons. However, even in the
411 presence of *para* RNAi we found a postnatal decrease in GF conduction time of
412 0.21ms (from 0.69 ± 0.04ms to 0.47 ± 0.03ms; fig. 3Ciii, table1), corresponding to
413 a postnatal speeding of only 47% (fig. 3Aii, table2), roughly half the postnatal
414 speeding found in control (80%; fig. 3Ai, 8, table2).

415 Since GF action potential conduction velocity was decreased upon
416 lowering the amount of Para channels, we hypothesized that conversely, an
417 upregulation of voltage-gated sodium channel expression will increase GF axonal
418 conduction velocity. Although *Drosophila* Para channels have been functionally
419 characterized in *Xenopus* oocytes (Lin et al., 2009), UAS-*para* transgenes have
420 so far not been successfully expressed in flies (Lin and Baines, 2015). Therefore,
421 we drove expression of a transgene encoding the bacterial sodium channels,
422 NaChBac, specifically in the GF (GF *split-Gal4*). Functional sodium current
423 through NaChBac expressed in *Drosophila* neurons and muscles has previously
424 been demonstrated (Luan et al., 2006; Nitabach et al., 2006). We predicted that
425 an increase in the total number of (bacterial + native) sodium channels will
426 increase axonal conduction velocity. Indeed, for both stages tested (1hPE and
427 24hPE), the latency in the GF-TTM pathway was significantly lower in flies
428 expressing the *NaChBac* transgene than in control ones (fig. 4Bi, 4Biii, 4Ci).
429 Again, given that expression was restricted to the GF interneuron, the latency
430 between TTMn and TTM remained unchanged following *NaChBac* transgene
431 expression (fig. 4Bii, 4Biv, 4Cii). Thus, in contrast to the increased axonal

conduction time upon *para* RNAi knockdown, the expression of extra sodium channels significantly decreased conduction time in the GF axon of 1hPE flies (0.52 ± 0.04ms vs 0.35 ± 0.02ms) and of 24hPE flies (0.29 ± 0.03ms vs 0.16 ± 0.03ms) (fig. 4Ciii, table1), and therefore, increased GF conduction speed (1.15 ± 0.09m/s vs 1.71 ± 0.10m/s) at 1hPE and (2.07 ± 0.21m/s vs 3.75 ± 0.70m/s) at 24hPE (fig. 4A, 4Civ). Therefore, with extra sodium (NaChBac) channel expression, the postnatal increase in action potential conduction velocity is further enhanced to 119% (fig. 4Aii, table2), as compared to the 80% enhancement in control (fig. 4Ai, 8, table2). To sum up, sodium channels control axonal conduction speed in the GF and may contribute to postnatal maturation.

We next tested possible contributions of other voltage-gated ion channels localized in the axon. It has recently been demonstrated that L-type calcium channels encoded by Dmca1D localize to motoneuron axons, where they augment high frequency firing (Kadas et al., 2017). Targeted *DmCa1D* RNAi knockdown, specifically in the GF, dramatically increased response latency in the GF-TTM pathway at both stages examined (fig. 5Bi, 5Biii, 5Ci). Given that the TTMn and its neuromuscular junction with TTM (TTMn/TTM) do not contribute to that change in response latency (fig. 5Bii, 5Biv, 5Cii), the data demonstrate that *DmCa1D* RNAi knockdown significantly increases GF axonal conduction time, both at 1hPE (0.52 ± 0.04ms vs 0.73 ± 0.05ms) and at 24hPE (0.29 ± 0.03ms vs 0.64 ± 0.04ms; fig. 5Ciii, table1). Noticeably, this corresponds to a decrease in GF axonal conduction speed of 40% (1.15 ± 0.09m/s vs 0.82 ± 0.06m/s) at 1hPE and a much higher decrease of 120% (2.07 ± 0.21m/s vs 0.94 ± 0.06m/s) at

455 24hPE (fig. 5A, 5Civ, table2). Consequently, in *DmCa1D* RNAi knockdown flies
456 postnatal speeding of GF axonal conduction velocity was reduced to just 15%
457 (fig. 5Aii, table2), as compared to 80% in control (fig. 4Ai, 8, table2). Hence, in
458 addition to reducing conduction speed at both stages tested, *DmCa1D* plays a
459 major role in postnatal conduction velocity speeding.
460
461
462 **Shaker and Slowpoke potassium channels control the GF conduction**
463 **velocity, but only Shaker contributes to its postnatal increment**
464
465 In addition to having identified two voltage-gated channels mediating inward
466 current that increase action potential conduction velocity, we also tested for
467 potential roles of potassium outward currents. We tested the *Drosophila*
468 homologs of the mammalian K_V1 and K_V4 voltage-gated potassium channels,
469 such as Shaker and Shal, and the BK channel homolog Slowpoke. In *Drosophila*
470 motoneurons, Shaker and Shal mediate fast activating, fast inactivating voltage-
471 gated potassium currents (Ryglewski, Duch, 2009), while Slowpoke underlies
472 transient calcium-activated potassium currents (Kadas et al., 2015). Expression
473 of each of these potassium channels was reduced by selective expression of the
474 respective UAS-RNAi transgenes specifically in the GF interneuron (von Reyn et
475 al., 2014).
476 Axonal localization of Shaker potassium channel in *Drosophila* DLM flight
477 MNs has previously been demonstrated by immunocytochemistry (Ryglewski,

Duch, 2009). Although light microscopy lacks sufficient spatial resolution to unambiguously assign labeled ion channel proteins to the membrane of an identified neuron *in situ*, high resolution confocal laser microscopy of UAS-tomato expressing GF axons in animals with endogenously GFP-tagged Shaker channels suggested that Shaker channels likely localize to the GF axonal membrane (figs. 6A-C). Representative projection views show the GF axons between the cervical connectives and their axon terminals in the thoracic neuromere, as well as many additional Shaker positive descending axons (fig. 6A). Single optical sections (0.3 µm section thickness) reveal patches of GFP tagged Shaker channels that co-localize with segments of UAS-tomato positive GF axonal membrane (figs. 6B, C), whereas the lumen of the large diameter GF axons is mostly devoid of Shaker label. This indicated functional Shaker channel localization to the GF axonal membrane.

Targeted RNAi knockdown of *shaker* (*sh*) in the GF significantly increased the latency in the GF-TTM pathway at both stages, though the effect is smaller at 1hPE (figs. 6Ei, 6Eiii, 6Fi). Again, motoneuron axonal conduction and neuromuscular transmission were not significantly affected by the expression of *sh* RNAi in the GF interneuron (fig. 6Eii, 6Eiv, 6Fii). *Sh* RNAi knockdown in the GF of 1hPE flies did not cause a statistically significant change in the GF conduction time (0.56ms ± 0.05ms vs 0.52 ± 0.04ms of control; fig. 6Fiii, table1). By contrast, *sh* RNAi knockdown in the GF of 24hPE flies significantly enhanced the GF conduction time (0.29 ± 0.03ms vs 0.41 ± 0.04ms of controls fig. 6Fiii, table1). Consequently, *sh* RNAi knockdown decreased GF axonal conduction

speed significantly at 24hPE (2.07 ± 0.21m/s vs 1.46 ± 0.14m/s), but not at 1hPE (1.15 ± 0.09m/s vs 1.07 ± 0.10m/s) (fig. 6A, 6Fiv). Given that *sh* RNAi knockdown reduced GF conduction at 24hPE by 42%, but only by 7% at 1hPE (table2), postnatal conduction speeding was only 36% (fig. DAii, table2), as compared to 80% in control (fig. 6Di, table2).

Targeted RNAi knockdown of *shal* in the GF caused a small but statistically significant increase of the latency recorded in the GF-TTM pathway at 1hPE (fig. 7Bi, 7Biii, 7Ci), without affecting the latency between TTMn and TTM (fig. 7Bii, 7Biv, 7Cii). By contrast, it did not significantly affect response latency of the GF-TTM pathway at 24hPE (fig. 7Bi, 7Biii, 7Ci). Similar to *sh* RNAi knockdown, the almost negligible increase in response latency in the GF-TTM pathway at 1hPE did not account for a statistically significant increase in the GF conduction time (fig. 7Ciii). Indeed, *shal* RNAi knockdown had only small effects on GF conduction velocity, a 6% at decreases at 1hPE (1.15 ± 0.09m/s vs 1.09 ± 0.06m/s) and a 14% decrease at 24hPE (2.07 ± 0.21m/s vs 1.82 ± 0.17m/s) (fig. 7A, 7Civ, table2). Therefore, Shal RNAi knockdown lowered postnatal speeding in GF conduction velocity only minimally, from 80% in controls (fig. 7Ai, 8, table2) to 67 % (67%; fig. 7Aii, table2).

Finally, RNAi knockdown of *slowpoke* (or *slo*) significantly increased GF-TTM pathway latency (fig. 8Bi, 8Biii, 8Ci) and axonal conduction time in the GF (fig. 8Ciii) at both stages tested (1hPE and 24hPE). Again, TTMn to TTM was not affected (fig. 8Bii, 8Biv, 8Cii) by *slo* RNAi knockdown in the GF. Given that *slo* RNAi exerted a slightly stronger effect at 24hPE than at 1hPE (56% decrease in

the GF conduction speed at 24hPE vs 35% at 1hPE; table2), the postnatal speeding of the GF conduction velocity in the presence of *slo* RNAi knockdown was reduced from 80% in control to 56% with *slo* RNAi expression (fig. 8A, 8Civ, 8, table2).

In summary, Shaker voltage-gated and Slowpoke calcium-activated potassium channels significantly increase axonal conduction velocity in the GF. However, in the presence of constant RNAi expression, postnatal speeding of the GF axonal conduction is affected much stronger with *sh* RNAi than with *slo* RNAi (see fig. 6A vs 8A). Knockdown of *para* reduces postnatal speeding to a similar amount as *sh* RNAi (see fig. 3A vs 6A). By contrast, targeted expression of *Dmca1D* RNAi eliminates postnatal speeding of axonal conduction velocity almost completely (see fig. 5A). In sum, postnatal upregulation of both Shaker outward and sodium inward current likely contributes to the postnatal increase of the GF axonal conduction speed, but up-regulation of L-type calcium channels seems most important.

DISCUSSION (1750 words)

AP conduction velocity in the GF interneuron increases postnatally

We show that information transfer through the *Drosophila* GFS becomes significantly faster during the first 24h of adult life. We ruled out functional changes in the PSI and/or the PSI/MN synapse, because these contribute only in the GF-DLM pathway, but both GFS branches showed similar decreases in response latency. This is in accord with previous findings that electrical (GF to TTMn, GF to PSI; Phelan et al., 1996; Jacobs et al., 2000) and chemical (PSI to MN1-5; Allen et al., 2006) synapse formation are completed during pupal stages. We also ruled out postnatal changes of MNs or neuromuscular synapses, because muscle response latencies to MN firing remained unaltered, and MN axons expand over the developing DLM muscles already by ~10h APF (Fernandes, Keshishian, 1996, 1998; Consoulas et al., 2002). Consequently, decreased response latency is caused by an 80% increase in GF axonal conduction velocity from 1.15 ± 0.09m/s at 1hPE to 2.07 ± 0.21m/s at 24PE. Although AP travel time through the GF axon is decreased by only 0.2ms, at the scale of a fruit fly this might be relevant. For a threat approaching with ~30km/h (roughly the speed of a frog tongue) 0.2ms provide an advantage of 1.6mm, more than half a fly's body length.

Axonal conduction velocity can be increased by enlarging axon diameter, improving plasma membrane insulation by myelination (Hartline, Colman, 2007; Fitzgerald, 1985; Fulton, 1987), or by adjusting ion channel expression levels, or by modifying channel properties (see below). First, although glial wrapping may affect conduction velocity in unmyelinated invertebrate axons (Dutta et al., 2016), we judge this mechanism unlikely, because mature GF conduction velocity is ~2m/s, comparable to vertebrate unmyelinated C-fibers. Second, GF morphological maturation is reportedly completed during pupal life (Allen et al., 1998), and we experimentally ruled out postnatal increases in outer axon diameter by CLSM. Therefore, we hypothesized changes in ion channel expression or in ion channel function to underlie postnatal conduction velocity increases. Postnatal changes in sodium and potassium currents are reported in rat optic nerve (Foster et al., 1982). In trigeminal ganglion sensory neuron (Aδ) postnatal conduction velocity increases are accompanied by a sharpening of AP shape (Cabanes et al., 2002). GF action potentials depend on sodium inward and potassium currents (Tanouye et al., 1981; Tanouye and Ferrus, 1985; von Reyn et al., 2014). Therefore, we first tested the role of fast sodium channels.

Increased sodium channel expression is required for GF postnatal speeding

591 Moderate RNAi knock-down of *para* (*DmNa$_v$*) decreased GF axonal conduction
592 velocity. Similarly, in unmyelinated axons innervating the rat cranial meninges,
593 reduced extracellular sodium concentrations or low doses of sodium channel
594 blockers decrease conduction velocity (De Col et al., 2008). By contrast,
595 overexpressing of bacterial sodium channels (NaChBac) increased GF axonal
596 conduction velocity. Since voltage-gated sodium channels mediate the rising
597 phase of the AP via positive feedback (Catterall, 2000), increased channel
598 numbers likely accelerate depolarization speed. Conversely, a faster
599 depolarization may accelerate sodium channel inactivation and thus increase
600 repolarization speed.
601 Reducing sodium channel expression affected GF conduction velocity in mature
602 flies significantly stronger than in newly eclosed ones. Therefore, the GF likely
603 becomes equipped with a larger number of fast sodium channels during the first
604 day of adult life. Alternatively, axonal conductance velocity could be regulated by
605 the expression of different sodium channel isoforms. A variety of Para splice
606 variants with different activation/inactivation kinetics exist (Olson et al., 2008; Lin
607 et al., 2009), and sodium current amplitude is affected by activity dependent
608 regulation of *para* mRNA levels and translation (Baines et al., 2001; Baines,
609 2003; Mee et al., 2004; Murano et al., 2008).
610 Similarly, in mammals, the ten genes (*SCN1A-SCN11A*; Goldin, 2001) encoding
611 sodium channel *α*-subunits show differential expression patterns during postnatal
612 maturation. Although it is known that the expression of TTX sensitive, fast Na$_v$1.6
613 and Na$_v$1.7 channels increases postnatally (Felts et al., 1997), while the

614 expression of TTX resistant, slower kinetics $Na_v1.8$ and $Na_v1.9$ channels peaks
615 earlier (Benn et al., 2001), a direct link to postnatal adjustments of conduction
616 velocities has not been made. In rat DRG, TTX resistant sodium channels may
617 contribute to the slow conduction velocity of unmyelinated C fibers (Ogata,
618 Tatebayashi, 1992).
619 Therefore, especially in non-myelinated axons the regulation of ion channel
620 expression seems to provide an effective means to adjust conduction velocity.
621 However, despite our finding that overexpression of bacterial sodium channels
622 increased conduction velocity, whereas reduction of para transcript by RNAi
623 reduced conduction velocity, we cannot rule that normal postnatal speeding may
624 be caused by additional mechanisms, such as the expression of accessory
625 subunits, differential splicing, or channel phosphorylation. Auxiliary subunits of
626 voltage gated ion channels can increase sodium channel functional diversity and
627 affect channel biophysical properties as well as trafficking and surfacing (Tseng
628 et al., 2007). Furthermore, channels expression and function are also regulated
629 by phosphorylation (Scheuer, 2011). Therefore, in addition to postnatal increases
630 of channel expression levels multiple additional mechanisms could in principle
631 increase GF axonal conduction velocity during the first day post eclosion. A direct
632 proof for increased sodium channel expression levels as the cause for GF
633 speeding would require single cell qRT-PCR of FISH.
634
635 **L-type calcium channels are required for postnatal increases in GF axonal**
636 **conduction velocity**

637

638 Our data indicate that sodium channels account only partially for GF axonal
639 conduction velocity increases. Targeted RNAi knockdown of *DmCa1D* L-type
640 calcium channels in the GF strongly decreased axonal conduction velocity at
641 both stages tested, and it abolished postnatal speeding almost completely. An
642 acute function of Dmca1D in fast AP conduction is difficult to reconcile with the
643 slow activation kinetics of most L-type channels (Mermelstein et al., 2000;
644 Yasuda et al., 2003). But note that L-type channel activation kinetics can be
645 altered by alternative splicing and auxiliary subunits (Birnbaumer et al. 1998;
646 Lipscombe 2002; Liu et al. 2003). Ten different Dmca1D isoforms are annotated,
647 and *Drosophila* HVA channels interact with auxillary β- and α2δ subunits. In larval
648 MNs calcium influx through Dmca1D indirectly reduces AP duration, rise and
649 decay times, and refractory period (Kadas et al., 2017), parameters which vary
650 inversely with conduction velocity in mammalian unmyelinated fibers (Paintal,
651 1967; Swadlow and Waxman, 1976). Therefore, axonal L-Type channels may
652 acutely increase GF conduction velocity.
653 Alternatively, activity dependent calcium influx through L-type channels may
654 regulate the expression levels of other ion channels (Flavell, Greenberg, 2008),
655 but this possibility is difficult to reconcile with the much stronger effect of
656 Dmca1D RNAi at 24h as compared to 1h post eclosion. However, a reduction of
657 Dmca1D expression by targeted RNAi expression critically counteracts the
658 normal increases in GF conduction velocity. Postnatal regulation of L-type
659 channel expression has also been reported in spinal cord (Jiang et al., 1999) and

sinoatrial node (Protas et al., 2001). At this point we cannot pinpoint whether Dmca1D current has a direct effect on conduction velocity, or whether calcium influx through Dmca1D channels alters the transcriptional level or properties of other ion channels, thus affecting GF conduction velocity indirectly. Ideally, one would measure expression levels of multiple channels with and without Dmca1D RNAi at both stages, but single cell qRT-PCR or FISH are beyond the scope of this study.

Shaker and BK channels increase GF conduction velocity and postnatal speeding

Outward potassium currents play crucial roles in limiting sodium channel inactivation or promoting de-inactivation (Baranauskas, 2007). In mammals and *Drosophila*, the fast AP afterhyperpolarization depends on A-type and BK potassium channels (Lancaster, Nicoll, 1987; Sah, Faber, 2002; Kadas et al., 2015). In the GF targeted RNAi knockdown of different potassium channels had different effects (table 2): Shal-RNAi (Kv4 homolog) had only small effects on conduction velocity and speeding. Slo-RNAi (BK homolog) reduced conduction velocity at both stages and reduced speeding by ~25 %. Shaker-RNAi (Kv1 homolog) reduced axonal conduction speed only in mature flies, thus limiting postnatal speeding. Shaker channels localize to the axons of *Drosophila* central neurons (Rogero et al., 1997), motoneurons (Ryglewski and Duch, 2009), and

likely also the GF axonal membrane (this study). In Shaker mutants APs recorded from the GF axon showed a prolonged repolarization (Tanouye et al., 1981; Tanouye and Ferrus, 1985). Slowpoke channels sharpen AP shape and shorten refractory period in *Drosophila* motoneurons (Kadas et al., 2015, 2017). Hence, Shaker and Slo are candidates for increasing GF axonal conduction velocity.

Given that *shaker* RNAi knockdown affects GF axonal conduction velocity at 24hPE but not at 1hPE, it seems likely that Shaker channel expression and localization to the GF axonal membrane is upregulated during the first day of adult life. Postnatal up-regulation of Shaker has also been described in rat neocortical and TG neurons, sympathetic neurons and in mouse hippocampus (Grosse et al., 2000; Seifert at al., 1999; McFarlane, Cooper, 1992; Bordey Sontheimer, 1997; Guan et al., 2011). However, on the level of immunocytochemistry for Shaker channels that were endogenously tagged with GFP, we could not find any evidence for a significant upregulation of Shaker protein levels, neither in the GF axonal membrane nor in neighboring descending axons. One possible explanation is that newly emerged flies (1hPE) lack auxiliary subunits (e.g. hyperkinetic) that render Shaker channel functional, or that other co-factors increase Shaker current through a given amount of channels during the first day of adult life. Although the precise mechanism requires further study, our data show that postnatal regulation of Shaker is required for postnatal increases of AP conduction velocity in the GF.

In sum, fast sodium current through Para channels, L-type calcium current through Dmca1D channels as well as A-type potassium current through Shaker and BK current through Slowpoke channels all increase axonal AP conduction velocity, most likely through AP sharpening. Postnatal regulation of either the expression levels (including appropriate trafficking to plasma membrane) or the function of these channels during the first day of adult life co-operatively increases AP conduction velocity by 80%, but the relative contributions of each channel are different. Regulating the expression levels and/ or properties of axonal ion channels provides a valuable means for increasing the speed of information transfer in unmyelinated axons, and thus, is likely a critical factor in invertebrate nervous system development and evolution. Therefore, direct measures of transcript levels or studies of mechanisms (e.g. differential splicing, post-translational modification, auxiliary subunits) controlling ion channel function, during postnatal maturation, will be needed to discriminate among these possibilities. By contrast, in the vertebrate NS myelination provides a more effective means, and thus mature conduction velocity of the unmyelinated GF remains about 20-60 times slower than that of vertebrate Aβ sensory axons and α motoneurons, despite roughly similar diameters.

REFERENCES

Allen MJ, Murphey RK (2007) The chemical component of the mixed GF-TTMn synapse in *Drosophila melanogaster* uses acetylcholine as its neurotransmitter. Eur J Neurosci 26:439-445.

Allen MJ, Drummond JA, Moffat KG (1998) Development of the giant fiber neuron of *Drosophila melanogaster*. J Comp Neurol 397:519-531.

Allen MJ, Shan X, Caruccio P, Froggett SJ, Moffat KG, Murphey RK (1999) Targeted expression of truncated glued disrupts giant fiber synapse formation in *Drosophila*. J Neurosci 19:9374-9384.

Allen MJ, Godenschwege TA, Tanouye MA, Phelan P (2006) Making an escape: development and function of the *Drosophila* giant fibre system. Semin Cell Dev Biol 17:31-41.

Baines RA (2003) Postsynaptic protein kinase A reduces neuronal excitability in response to increased synaptic excitation in the *Drosophila* CNS. J Neurosci 23:8664–8672.

Baines RA, Uhler JP, Thompson A, Sweeney ST, Bate M (2001) Altered electrical properties in *Drosophila* neurons developing without synaptic transmission. J Neurosci 21:1523–1531.

Baranauskas G (2007). Ionic channel function in action potential generation: current perspective. Mol Neurobiol 35:129-150.

Barnea-Goraly N, Menon V, Eckert M, Tamm L, Bammer R, Karchemskiy A, Dant CC, Reiss AL (2005) White matter development during childhood and adolescence: a cross-sectional diffusion tensor imaging study. Cereb Cortex 15: 1848-1854.

Benn SC, Costigan M, Tate S, Fitzgerald M, Woolf CJ (2001) Developmental expression of the TTX-resistant voltage-gated sodium channels $Na_v1.8$ (SNS) and $Na_v1.9$ (SNS2) in primary sensory neurons. J Neurosci 21:6077-6085.

Birnbaumer L, Qin N, Olcese R, Tareilus E, Platano D, Costantin J, Stefani E (1998) Structures and functions of calcium channel beta subunits. J Bioenerg Biomembr 30:357-375.

Blagburn JM, Alexopoulos H, Davies JA, Bacon JP (1999) Null mutation in shaking-B eliminates electrical, but not chemical, synapses in the *Drosophila* giant fiber system: a structural study. J Comp Neurol 404:449-458.

772 Bordey A, Sontheimer H (1997) Postnatal development of ionic currents in rat
773 hippocampal astrocytes in situ. J Neurophysiol 78:461-477.

774 Cabanes C, López de Armentia M, Viana F, Belmonte C (2002) Postnatal
775 changes in membrane properties of mice trigeminal ganglion neurons. J
776 Neurophysiol 87:2398-2407.
777
778 Catterall WA (2000) From ionic currents to molecular mechanisms: the structure
779 and function of voltage-gated sodium channels. Neuron 26:13–25.
780
781 Consoulas C, Restifo LL, Levine RB (2002) Dendritic remodeling and growth of
782 motoneurons during metamorphosis of *Drosophila melano*gaster. J Neurosci
783 22:4906–4917.

784 De Col R, Messlinger K, Carr RW (2008) Conduction velocity is regulated by
785 sodium channel inactivation in unmyelinated axons innervating the rat cranial
786 meninges. J Physiol 586:1089–1103.

787 Duncan CE, Webster MJ, Rothmond DA, Bahn S, Elashoff M, Shannon Weickert
788 C (2010) Prefrontal $GABA_A$ receptor α-subunit expression in normal postnatal
789 human development and schizophrenia. J Psychiatr Res 44:673-681.

790 Dutta S, Rieche F, Eckl N, Duch C, Kretzschmar D (2016) Glial expression of
791 Swiss cheese (SWS), the *Drosophila* orthologue of neuropathy target esterase
792 (NTE), is required for neuronal ensheathment and function. Dis Model Mech
793 9:283-294.

794 Engel JE, Wu C-F (1992) Interactions of membrane excitability mutations
795 affecting potassium and sodium currents in the flight and giant fiber escape
796 systems of *Drosophila*. J Comp Physiol A Neuroethol Sens Neural Behav Physiol
797 171:93-104.

798 Felts PA, Yokoyama S, Dib-Hajj S, Black JA, Waxman SG (1997) Sodium
799 channel alpha-subunit mRNAs I, II, III, NaG, Na6 and hNE (PN1): different
800 expression patterns in developing rat nervous system. Brain Res Mol Brain Res
801 45:71-82.

802 Feng G, Deák P, Chopra M, Hall LM (1995) Cloning and functional analysis of
803 TipE, a novel membrane protein that enhances *Drosophila* para sodium channel
804 function. Cell 82:1001–1011.

805 Fernandes JJ, Keshishian H (1996) Patterning the dorsal longitudinal flight
806 muscles (DLM) of *Drosophila*: insights from the ablation of larval scaffolds.
807 Development 122: 3755-3763.

808 Fernandes JJ, Keshishian H (1998) Nerve-muscle interactions during flight
809 muscle development in *Drosophila*. Development 125: 1769-1779.

Fitzgerald M (1985) The post-natal development of cutaneous afferent fibre input and receptive field organization in the rat dorsal horn. J Physlol 364:1-18.

Fitzgerald M (1987) Cutaneous primary afferent properties in the hind limb of the neonatal rat. J Physlol 383:79-92.

Flavell SW, Greenberg ME (2008) Signaling mechanisms linking neuronal activity to gene expression and plasticity of the nervous system. Annu Rev Neurosci 31:563-590.

Foster RE, Connors BW, Waxman SG (1982) Rat optic nerve*:* electrophysiological*,* pharmacological and anatomical studies during development*.* Brain Res 255:371-386.

Fulton BP (1986) Postnatal changes in active membrane properties of rat dorsal root ganglion neurons. J Physiol 377:80P.

Fulton BP (1987) Postnatal changes in conduction velocity and soma action potential parameters of rat dorsal root ganglion neurons. Neurosci Lett 73:125–130.

Gibson EM, Purger D, Mount CW, Goldstein AK, Lin GL, Wood LS, Inema I, Miller SE, Bieri G, Zuchero JB, Barres BA, Woo PJ, Vogel H, Monje M (2014) Neuronal activity promotes oligodendrogenesis and adaptive myelination in the mammalian brain. Science 344:1252304.

Goldin AL (2001) Resurgence of sodium channel research. Annu Rev Physiol 63:871-894.

Grosse G, Draguhn A, Höhne L, Tapp R, Veh RW, Ahnert-Hilger G (2000) Expression of K_v1 potassium channels in mouse hippocampal primary cultures: development and activity-dependent regulation. J Neurosci 20:1869-1882.

Guan D, Horton LR, Armstrong WE, Foehring RC (2011) Postnatal development of A-type and K_v1- and K_v2-mediated potassium channel currents in neocortical pyramidal neurons. J Neurophysiol 105:2976-2988.

Hammond S, O'Shea M (2007) Escape flight initiation in the fly. J Comp Physiol A Neuroethol Sens Neural Behav Physiol 193:471-476.

Hartline DK, Colman DR (2007) Rapid conduction and the evolution of giant axons and myelinated fibers. Curr Biol 17:R29-35.

Hodgkin AL (1954) A note on conduction velocity. J Physiol 125:221–224.

Ikeda K, Koenig JH (1988) Morphological identification of the motor neurons innervating the dorsal longitudinal flight muscle of *Drosophila melanogaster*. J Comp Neurol 273:436-444.

Jaaro-Peled H, Hayashi-Takagi A, Seshadri S, Kamiya A, Brandon NJ, Sawa A (2009) Neurodevelopmental mechanisms of schizophrenia: understanding disturbed postnatal brain maturation through neuregulin-1-ErbB4 and DISC1. Trends Neurosci 32:485-495.

Jacobs K, Todman MG, Allen MJ, Davies JA, Bacon JP (2000) Synaptogenesis in the giant-fibre system of *Drosophila*: interaction of the giant fibre and its major motorneuronal target. Development 127:5203-5212.

Jiang Z, Rempel J, Li J, Sawchuk MA, Carlin KP, Brownstone RM (1999) Development of L-type calcium channels and a nifedipine-sensitive motor activity in the postnatal mouse spinal cord. Eur J Neurosci 11:3481-3487.

Kaas GA, Kasuya J, Lansdon P, Ueda A, Iyengar A, Wu CF, Kitamoto T (2016) Lithium-Responsive Seizure-Like Hyperexcitability Is Caused by a Mutation in the Drosophila Voltage-Gated Sodium Channel Gene paralytic. eNeuro 3(5) e0221-16.

Kadas D, Tzortzopoulos A, Skoulakis EM, Consoulas C (2012) Constitutive activation of Ca2+/calmodulin-dependent protein kinase II during development impairs central cholinergic transmission in a circuit underlying escape behavior in *Drosophila*. J Neurosci 32:170-182.

Kadas D, Ryglewski S, Duch C (2015) Transient BK outward current enhances motoneurone firing rates during *Drosophila* larval locomotion. J Physiol 593:4871-4888.

Kadas D, Klein A, Krick N, Worrell JW, Ryglewski S, Duch C (2017) Dendritic and axonal L-Type calcium channels cooperate to enhance motoneuron firing output during *Drosophila* larval locomotion. J Neurosci 37:10971-10982.

Kano M, Watanabe T, Uesaka N, Watanabe M (2018) Multiple Phases of Climbing Fiber Synapse Elimination in the Developing. Cerebellum.

King DG, Wyman RJ (1980) Anatomy of the giant fibre pathway in *Drosophila*. I. Three thoracic components of the pathway. J Neurocytol 9:753–770.

Koenig JH, Ikeda K (2005) Relationship of the reserve vesicle population to synaptic depression in the tergotrochanteral and dorsal longitudinal muscles of *Drosophila*. J Neurophysiol 94:2111-2119.

881 Koto M, Tanouye MA, Ferrus A, Thomas JB, Wyman RJ (1981) The morphology
882 of the cervical giant fiber neuron of *Drosophila*. Brain Res 221:213-217.
883
884 Lancaster B & Nicoll RA (1987) Properties of two calcium-activated
885 hyperpolarizations in rat hippocampal neurones. J Physiol 389:187–203.

886 Lin WH, Baines RA (2015) Regulation of membrane excitability: a convergence
887 on voltage-gated sodium conductance. Mol Neurobiol 51:57-67.

888 Lin WH, Wright DE, Muraro NI, Baines RA (2009) Alternative splicing in the
889 voltage-gated sodium channel DmNav regulates activation, inactivation, and
890 persistent current. J Neurophysiol 102:1994-2006.

891 Lipscombe D, Pan JQ, Gray AC (2002) Functional diversity in neuronal voltage-
892 gated calcium channels by alternative splicing of $Ca_v\alpha_1$. Mol Neurobiol 26:21-44.

893 Lipscombe D, Helton TD, Xu W (2004) L-type calcium channels: the low down. J
894 Neurophysiol 92:2633-2641.

895 Liu G, Hilliard N, Hockerman GH (2004) $Ca_v1.3$ is preferentially coupled to
896 glucose-induced $[Ca^{2+}]i$ oscillations in the pancreatic β cell line INS-1. Mol
897 Pharmacol 65:1269-1277.

898 Luan H, Lemon WC, Peabody NC, Pohl JB, Zelensky PK, Wang D, Nitabach MN,
899 Holmes TC, White BH (2006) Functional dissection of a neuronal network
900 required for cuticle tanning and wing expansion in *Drosophila*. J Neurosci 26:573-
901 584.

902 Maffei A, Turrigiano (2008) The age of plasticity: developmental regulation of
903 synaptic plasticity in neocortical microcircuits. Prog Brain Res 196:211-223.

904 McFarlane S, Cooper E (1992) Postnatal development of voltage-gated K
905 currents on rat sympathetic neurons. J Neurophysiol 67:1291-1300.

906 Mee CJ, Pym EC, Moffat KG, Baines RA (2004) Regulation of neuronal
907 excitability through pumilio-dependent control of a sodium channel gene. J
908 Neurosci 24:8695– 8703.

909 Mermelstein PG, Bito H, Deisseroth K, Tsien RW (2000) Critical dependence of
910 cAMP response element-binding protein phosphorylation on L-type calcium
911 channels supports a selective response to EPSPs in preference to action
912 potentials. J Neurosci 20:266-273.

913 Moore JW, Joyner RW, Brill MH, Waxman SD, Najar-Joa M (1978) Simulations
914 of conduction in uniform myelinated fibers. Relative sensitivity to changes in
915 nodal and internodal parameters. Biophys J 21:147–160.

916
917 Muraro NI, Weston AJ, Gerber AP, Luschnig S, Moffat KG, Baines RA (2008)
918 Pumilio binds para mRNA and requires Nanos and Brat to regulate sodium
919 current in *Drosophila* motoneurons. J Neurosci 28:2099–2109.
920

921 Nitabach MN, Wu Y, Sheeba V, Lemon WC, Strumbos J, Zelensky PK, White
922 BH, Holmes TC (2006) Electrical hyperexcitation of lateral ventral pacemaker
923 neurons desynchronizes downstream circadian oscillators in the fly circadian
924 circuit and induces multiple behavioral periods. J Neurosci 26:479-489.

925 Ogata N, Tatebayashi H (1992) Ontogenic development of the TTX-sensitive and
926 TTX-insensitive Na^+ channels in neurons of the rat dorsal root ganglia. Brain Res
927 Dev Brain Res 65:93-100.

928 Olson RO, Liu Z, Nomura Y, Song W, Dong K (2008) Molecular and functional
929 characterization of voltage-gated sodium channel variants from *Drosophila*
930 *melanogaster*. Insect Biochem Mol Biol 38:604–610.

931 Paintal AS (1967) A comparison of the nerve impulses of mammalian non-
932 medullated nerve fibres with those of the smallest diameter medullated fibres. J
933 Physiol 193:523-533.

934 Peters A, Muir AR (1959) The relationship between axons and Schwann cells
935 during development of peripheral nerves in the rat. Q J Exp Physiol Cogn Med
936 Sci 44:117-130.

937 Pézier AP, Jezzini SH, Bacon JP, Blaqburn JM (2016) Shaking B Mediates
938 Synaptic Coupling between Auditory Sensory Neurons and the Giant Fiber of
939 *Drosophila melanogaster*. PLoS One 11:e0152211.

940 Phelan P, Nakagawa M, Wilkin MB, Moffat KG, O'Kane CJ, Davies JA, Bacon JP
941 (1996) Mutations in shaking-B prevent electrical synapse formation in the
942 *Drosophila* giant fiber system. J Neurosci 16:1101-13.

943 Protas L, DiFrancesco D, Robinson RB (2001) L-type but not T-type calcium
944 current changes during postnatal development in rabbit sinoatrial node. Am J
945 Physiol Heart Circ Physiol 281:H1252-H1259.

946 Pun RY, Rolle IJ, Lasarge CL, Hosford BE, Rosen JM, Uhl JD, Schmeltzer SN,
947 Faulkner C, Bronson SL, Murphy BL, Richards DA, Holland KD, Danzer SC
948 (2012) Excessive activation of mTOR in postnatally generated granule cells is
949 sufficient to cause epilepsy. Neuron 75:1022-1034.

950 Rogero O, Hämmerle B, Tejedor FJ (1997) Diverse expression and distribution of
951 Shaker potassium channels during the development of the *Drosophila* nervous
952 system. J Neurosci 17:5108-5118.

953 Ryglewski S, Duch C (2009) Shaker and Shal mediate transient calcium-
954 independent potassium current in a *Drosophila* flight motoneuron. J
955 Neurophsysiol 102:3673-3688.

956 Sah P & Faber ES (2002) Channels underlying neuronal calcium-activated
957 potassium currents. Prog Neurobiol 66:345-353.
958

959 Schaefer JE, Worrell JW, Levine RB (2010) Role of intrinsic properties
960 in Drosophila motoneuron recruitment during fictive crawling. J Nerurophysiol
961 104:1257-1266.

962 Scharfman HE, McCloskey DP (2009) Postnatal neurogenesis as a therapeutic
963 target in temporal lobe epilepsy. Epilepsy Res 85:150-161.

964 Scheuer T (2011) Regulation of sodium channel activity by phosphorylation.
965 Semin Cell Dev Biol 22:160-165.

966 Schützler N, Girwert C, Hügli I, Mohana G, Roignant JY, Ryglewski S, Duch C
967 (2019) Tyramine action on motoneuron excitability and adaptable
968 tyramine/octopamine ratios adjust Drosophila locomotion to nutritional state.
969 PNAS 116(9):3805-3810.

970 Seifert G, Kuprijanova E, Zhou M, Steinhäuser C (1999) Developmental changes
971 in the expression of Shaker- and Shab-related K^+ channels in neurons of the rat
972 trigeminal ganglion. Brain Res Mol Brain Res 74:55-68.

973 Sun YA, Wyman RJ (1996) Passover eliminates gap junctional communication
974 between neurons of the giant fiber system in *Drosophila*. J Neurobiol 30:340-348.
975

976 Sun YA, Wyman RJ (1997) Neurons of the *Drosophila* giant fiber system: I.
977 Dorsal longitudinal motor neurons. J Comp Neurol 387:157-66.

978 Swadlow HA, Waxman SG (1976) Variations in conduction velocity and
979 excitability following single and multiple impulses of visual callosal axons in the
980 rabbit. Exp Neurol 53:128-150.

981 Tanouye MA, Wyman R (1980) Motor outputs of giant nerve fiber in Drosophila. J
982 Neurophysiol 44:405-421.

983 Tanouye MA, Ferrus A (1985) Action potentials in normal and Shaker mutant
984 *Drosophila*. J Neurogenet 2: 253-271.

985 Tanouye MA, Ferrus A, Fujita SC (1981) Abnormal action potentials associated
986 with the Shaker complex locus of *Drosophila*. Proc Natl Acad Sci U S A 78:6548-
987 6552.

988 Trimarchi JR, Schneiderman AM (1993) Giant fiber activation of an intrinsic
989 muscle in the mesothoracic leg of *Drosophila melanogaster*. J Exp Biol 177:149-
990 167.

991 Tseng TT, McMahon AM, Johnson VT, Mangubat EZ, Zahm RJ, Pacold ME,
992 Jakobsson E (2007) Sodium channel auxiliary subunits. J Mol Microbiol
993 Biotechnol 12:249-262.

994 Viana F, Bayliss DA, Berger AJ (1994) Postnatal changes in rat hypoglossal
995 motoneuron membrane properties. Neuroscience 59:131-148.

996 Vincent A, Tell F (1997) Postnatal changes in electrophysiological properties of
997 rat nucleus tractus solitarii neurons. Eur J Neurosci 9:1612-1624.

998 von Reyn CR, Breads P, Peek MY, Zheng GZ, Williamson WR, Yee AL,
999 Leonardo A, Card GM (2014) A spike-timing mechanism for action selection. Nat
1000 Neurosci 17:962-970.

1001 Webb SJ, Monk CS, Nelson CA (2001) Mechanisms of postnatal neurobiological
1002 development: implications for human development. Dev Neuropsychol 19:147-
1003 171.

1004 Yasuda R, Sabatini BL, Svoboda K (2003) Plasticity of calcium channels in
1005 dendritic spines. Nat Neurosci 6:948-955.

1006 Zhou FM, Hablitz JJ (1996) Postnatal development of membrane properties of
1007 layer I neurons in rat neocortex. J Neurosci 16:1131-1139.

1008

1009

1010 **FIGURE LEGENDS**

1011

1012 **Figure 1.** The GF axonal conduction velocity increases 80% during postnatal
1013 maturation. ***A,*** GFS schematic depiction at 1hPE (***Ai***) and 24hPE (***Aii***) control
1014 flies. Average latency ± SEM for GF-DLM5-6, GF-TTM, MN5-DLM5-6 and TTMn-
1015 TTM branches are indicated between dotted lines. Lower boxes on GF indicate
1016 the latency in the GF axon. Upper boxes on GF indicates the GF axonal speed.
1017 The percentage of the GF speeding (80%) during the first day of the fly life is

presented in the gray-black arrow. ***B,*** 10 overlapping sweeps of action potentials recorded from DLM5-6 muscles, after GF (***Bi***) or MN5 (***Bii***) stimulation, and from TTM muscle, after GF (***Biii***) or TTMn (***Biv***) stimulation, at 1hPE (gray) and 24hPE (black) flies. Times above double arrows indicate the latency, which is measured as the interval of time between the stimulus artifact (black arrow) and the onset of the initial phase of muscle potential (white arrow). Underlined time values show the difference in latency measurements between the two stages. ***C,*** Latency measurements in the GF-DLM5-6 and GF-TTM pathways (***Ci***), in the MN5-DLM5-6 and TTMn-TTM sub-pathways (***Cii***), in the GF axon (***Ciii***) and measurements of the GF axonal speed (***Civ***), at 1hPE (50% black)), 12hPE (70% black) and 24hPE or 48hPE (black) flies. Underlined time values between dotted arrows indicate the latency difference between1hPE and 24hPE. Data are shown as means ± SEM (*Ci-iii*). Dots on box plots showcase the measurements from individual flies (*Civ*). Asterisks indicate p values from one-way ANOVA with posthoc Dunnett's tests (*p < 0.05, **p < 0.01, ***p < 0.001, ****p < 0.0001). GFS, Giant Fiber System; GF, Giant Fiber; 1hPE, 1 hour Post-Eclosion; 24hPE, 24 hours Post-Eclosion; PSI, Peripherally Synapsing Interneuron; MN5, Motoneuron 5; DLM, Dorsal Longitudinal Muscle; TTM; Tergotrochanteral Muscle; St, Stimulation site, Re, Recording site; S, stimulus; R, Record.

Figure 2. The GF axon diameter does not increase postnatally, and GFP-RNAi decreases GFP fluorescence similarly at 1h and 24h post eclosion. ***A,*** Representative confocal image stacks of the GF interneuron axons between the neck connectives and the terminals in the VNC at 1hPE (***A***) and at 24hPE (***B***). To avoid potential histology artifacts images were taken live in saline with a 60x water dipping lens from freshly dissected animals with UAS-cd4-tomato expression in the GF. White boxes indicate areas shown as selective enlargements in ***(Ai)*** and ***(Bi)***. ***C,*** Quantification from 14 axons at each stage shows that GF axon diameter is similar at 1hPE and 24hPE (p > 0.6, Students T-

test). VNC, Ventral Nerve Cord. ***(D-G)*** In comparison to control ***(D)*** targeted GFP RNAi knock down reduces GFP fluorescence at both stages tested, 24hPE ***(E)*** and 1hPE (F). ***(G)*** Quantification of mean gray levels in 8 bit tiff images of the GF axon (0-254 gray levels) reveals a significant reduction by about 70%, but no differences between both stages tested (ANOVA with Newman Keuls posthoc testing). ** indicates P < 0.01, n.s. indicates p > 0.3.

Figure 3. *Para*-RNAi decreases postnatal conduction velocity speeding in the GF. ***A,*** GF schematic depiction at 1hPE (gray) and 24hPE (black) in controls (***Ai***) as compared to 1hPE (orange) and 24hPE (red) in flies with *para* RNAi (***Aii***). GF axonal conduction velocity (dotted arrow) is given for each experimental group. The percentage of the GF postnatal speeding in control (gray-black arrow, 80%) is strongly reduced by *para* RNAi knockdown (orange-red arrow, 47%). ***B,*** Representative TTM muscle action potentials recorded after GF (***Bi***) or TTMn (***Bii***) stimulation at 1hPE (gray) and at 24hPE (black) in control flies as compared to *para* RNAi knockdown (***Biii,*** GF stimulation; **Biv,** TTMn stimulation) at 1hPE (orange) and at 24hPE (red). Times above double arrows and between dotted lines indicate the latency between GF (or TTMn) and TTM. Latency differences between stages are underlined for control and for *para* RNAi knockdown. ***C,*** Latency measurements in the GF-TTM pathway (***Ci***), in the TTMn-TTM sub-pathway (***Cii***), in the GF axon (***Ciii***) and measurements of the GF axonal speed (C***iv***), at 1hPE (gray) and 24hPE (black) in controls and at 1hPE (orange) and 24hPE (red) in flies expressing *para* RNAi transgene. Underlined times between dotted arrows indicate the latency difference between the two stages in control and *para* RNAi knockdown. Data are shown as means ± SEM (*Ci-iii*). Dots on box plots showcase the measurements from individual flies (*Civ*). Asterisks indicate p values from one-way ANOVA with posthoc Dunnett's tests (*p < 0.05, ***p < 0.001, ****p < 0.0001).

Figure 4. Expression of extra sodium channels (NaChBac) increases postnatal conduction velocity speeding in the GF. ***A,*** GF schematic depiction at 1hPE (gray) and 24hPE (black) in controls (***Ai***) as compared to 1hPE (light orange) and 24hPE (neon red) in flies expressing NaChBac channels (***Aii***). GF axonal conduction velocity (dotted arrow) is given for each experimental group. The percentage of the GF postnatal speeding in control (gray-black arrow, 80%) is strongly increased by NaChBac channels expression (light orange-neon red, 119%). ***B,*** Representative TTM muscle action potentials recorded after GF (***Bi***) or TTMn (***Bii***) stimulation at 1hPE (gray) and at 24hPE (black) in control flies as compared to flies expressing NaChBac channels (***Biii,*** GF stimulation; **Biv,** TTMn stimulation) at 1hPE (light orange) and at 24hPE (neon red). Times above double arrows and between dotted lines indicate the latency between GF (or TTMn) and TTM. Latency differences between stages are underlined for control and for NaChBac channels expression. ***C,*** Latency measurements in the GF-TTM pathway (***Ci***), in the TTMn-TTM sub-pathway (***Cii***), in the GF axon (***Ciii***) and measurements of the GF axonal speed (C***iv***), at 1hPE (gray) and 24hPE (black) in controls and at 1hPE (light orange) and 24hPE (neon red) in flies expressing *NaChBac* transgene. Underlined times between dotted arrows indicate the latency difference between the two stages in control and flies expressing NaChBac sodium channels. Data are shown as means ± SEM (*Ci-iii*). Dots on box plots showcase the measurements from individual flies (*Civ*). Asterisks indicate p values from one-way ANOVA with posthoc Dunnett's tests (**p < 0.01, ***p < 0.001, ****p < 0.0001).

Figure 5. *DmCa1D*-RNAi almost eliminates postnatal conduction velocity speeding in the GF. ***A,*** GF schematic depiction at 1hPE (gray) and 24hPE (black) in controls (***Ai***) as compared to 1hPE (cyan) and 24hPE (blue) in flies with

DmCa1D RNAi (***Aii***). GF axonal conduction velocity (dotted arrow) is given for each experimental group. The percentage of the GF postnatal speeding in control (gray-black arrow, 80%) is extremely reduced by *DmCa1D* RNAi knockdown (cyan-blue arrow, 15%). ***B,*** Representative TTM muscle action potentials recorded after GF (***Bi***) or TTMn (***Bii***) stimulation at 1hPE (gray) and at 24hPE (black) in control flies as compared to *DmCa1D* RNAi knockdown (***Biii,*** GF stimulation; **Biv,** TTMn stimulation) at 1hPE (cyan) and at 24hPE (blue). Times above double arrows and between dotted lines indicate the latency between GF (or TTMn) and TTM. Latency differences between stages are underlined for control and for *DmCa1D* RNAi knockdown. ***C,*** Latency measurements in the GF-TTM pathway (***Ci***), in the TTMn-TTM sub-pathway (***Cii***), in the GF axon (***Ciii***) and measurements of the GF axonal speed (C***iv***), at 1hPE (gray) and 24hPE (black) in controls and at 1hPE (cyan) and 24hPE (blue) in flies expressing *DmCa1D* RNAi transgene. Underlined time values between dotted arrows indicate the latency difference between the two stages in control and *DmCa1D* RNAi knockdown. Data are shown as means ± SEM (*Ci-iii*). Dots on box plots showcase the measurements from individual flies (*Civ*). Asterisks indicate p values from one-way ANOVA with posthoc Dunnett's tests (*p < 0.05, **p < 0.01, ***p < 0.001, ****p < 0.0001).

Figure 6. Shaker channels are localized in the GF axon and *Sh*-RNAi decreases postnatal conduction velocity speeding. ***A-Aii,*** Projection views of a representative confocal image stack from the GF with UAS-cd4-tomato expression (red) and Shaker channel expression as visualized by an endogenous GFP tag (green). Dotted white boxes in ***(Ai)*** indicate the areas which are selectively enlarged in ***(B)*** and in ***(C)*** and shown as z-projections of 1µm (3 optical sections). White arrowheads demark areas with overlap of patches of GF axonal membrane (red) and Shaker-GFP label. The GF axonal lumen is mostly devoid of Shaker-GFP label. ***D,*** GF schematic depiction at 1hPE (gray) and 24hPE (black) in controls (***Di***) as compared to 1hPE (violet) and 24hPE (purple) in flies with *Sh* RNAi (***Dii***). GF axonal conduction velocity (dotted

arrow) is given for each experimental group. The percentage of the GF postnatal speeding in control (gray-black arrow, 80%) is strongly reduced by *Sh* RNAi knockdown (violet-purple arrow, 36%). ***E,*** Representative TTM muscle action potentials recorded after GF (***Ei***) or TTMn (***Eii***) stimulation at 1hPE (gray) and at 24hPE (black) in control flies as compared to *Sh* RNAi knockdown (***Eiii,*** GF stimulation; **Eiv,** TTMn stimulation) at 1hPE (violet) and at 24hPE (purple). Times above double arrows and between dotted lines indicate the latency between GF (or TTMn) and TTM. Latency differences between stages are underlined for control and for *Sh* RNAi knockdown. ***F,*** Latency measurements in the GF-TTM pathway (***Fi***), in the TTMn-TTM sub-pathway (***Fii***), in the GF axon (***Fiii***), and measurements of the GF axonal speed (F***iv***), at 1hPE (gray) and 24hPE (black) in controls and at 1hPE (violet) and 24hPE (purple) in flies expressing *Sh* RNAi. Underlined times between dotted arrows indicate the latency difference between the two stages in control and *Sh* RNAi knockdown. Data are shown as means ± SEM (*Fi-iii*). Dots on box plots showcase the measurements from individual flies (*Fiv*). Asterisks indicate p values from one-way ANOVA with posthoc Dunnett's tests (*p < 0.05, ***p < 0.001, ****p < 0.0001).

Figure 7. *Shal*-RNAi does not affect postnatal conduction velocity speeding in the GF. ***A,*** GF schematic depiction at 1hPE (gray) and 24hPE (black) in controls (***Ai***) as compared to 1hPE (violet) and 24hPE (purple) in flies with *Shal* RNAi (***Aii***). GF axonal conduction velocity (dotted arrow) is given for each experimental group. The percentage of the GF postnatal speeding in control (gray-black arrow, 80%) is not significantly reduced by *Shal* RNAi knockdown (violet-purple arrow, 67%). ***B,*** Representative TTM muscle action potentials recorded after GF (***Bi***) or TTMn (***Bii***) stimulation at 1hPE (gray) and at 24hPE (black) in control flies as compared to *Shal* RNAi knockdown (***Biii,*** GF stimulation; **Biv,** TTMn stimulation) at 1hPE (violet) and at 24hPE (purple). Times above double arrows and between dotted lines indicate the latency between GF (or TTMn) and TTM. Latency differences between stages are underlined for control and for *Shal* RNAi knockdown. ***C,*** Latency measurements in the GF-TTM pathway (***Ci***), in the

TTMn-TTM sub-pathway (***Cii***), in the GF axon (***Ciii***) and measurements of the GF axonal speed (C***iv***), at 1hPE (gray) and 24hPE (black) in controls and at 1hPE (violet) and 24hPE (purple) in flies expressing *Shal* RNAi transgene. Underlined time values between dotted arrows indicate the latency difference between the two stages in control and *Shal* RNAi knockdown. Data are shown as means ± SEM (*Ci-iii*). Dots on box plots showcase the measurements from individual flies (*Civ*). Asterisks indicate p values from one-way ANOVA with posthoc Dunnett's tests (***p < 0.001, ****p < 0.0001).

Figure 8. *Slo*-RNAi affects slightly postnatal conduction velocity speeding in the GF ***A,*** GF schematic depiction at 1hPE (gray) and 24hPE (black) in controls (***Ai***) as compared to 1hPE (mint green) and 24hPE (green) in flies with *Slo* RNAi (***Aii***). GF axonal conduction velocity (dotted arrow) is given for each experimental group. The percentage of the GF postnatal speeding in control (gray-black arrow, 80%) is moderately reduced by *Slo* RNAi knockdown (mint green-green arrow, 56%). ***B,*** Representative TTM muscle action potentials recorded after GF (***Bi***) or TTMn (***Bii***) stimulation at 1hPE (gray) and at 24hPE (black) in control flies as compared to *Slo* RNAi knockdown (***Biii,*** GF stimulation; **Biv,** TTMn stimulation) at 1hPE (mint green) and at 24hPE (green). Times above double arrows and between dotted lines indicate the latency between GF (or TTMn) and TTM. Latency differences between stages are underlined for control and for *Slo* RNAi knockdown. ***C,*** Latency measurements in the GF-TTM pathway (***Ci***), in the TTMn-TTM sub-pathway (***Cii***), in the GF axon (***Ciii***) and measurements of the GF axonal speed (C***iv***), at 1hPE (gray) and 24hPE (black) in controls and at 1hPE (mint green) and 24hPE (green) in flies expressing *Slo* RNAi transgene. Underlined time values between dotted arrows indicate the latency difference between the two stages in control and *Slo* RNAi knockdown. Data are shown as means ± SEM (*Ci-iii*). Dots on box plots showcase the measurements from individual flies (*Civ*). Asterisks indicate p values from one-way ANOVA with posthoc Dunnett's tests (**p < 0.01, ***p < 0.001, ****p < 0.0001).

Table 1. Latency measurements in the GF-TTM pathways, in the TTMn-TTM sub-pathways and in the GF axon at 1hPE (gray) and 24hPE (black) control as compared to 1hPE and 24hPE in flies where genes encoding ion channels were expressed or knocked down specifically in the GF interneurons. The latency in the GF axon is estimated by subtracting the TTMn-TTM latency from the GF-TTM latency. Data are shown as means ± SEM. (n), number of preparation tested.

Table 2. % increase (+) or decrease (-) in GF axonal conduction speed due to targeted expression or knockdown of genes encoding ion channels in the GF interneurons at 1hPE (gray) and 24hPE (black) flies, or during the first day of the fly life (1-24hPE). Asterisks indicate p values from one-way ANOVA with posthoc Dunnett's tests (*p < 0.05, **p < 0.01, ***p < 0.001, ****p < 0.0001).

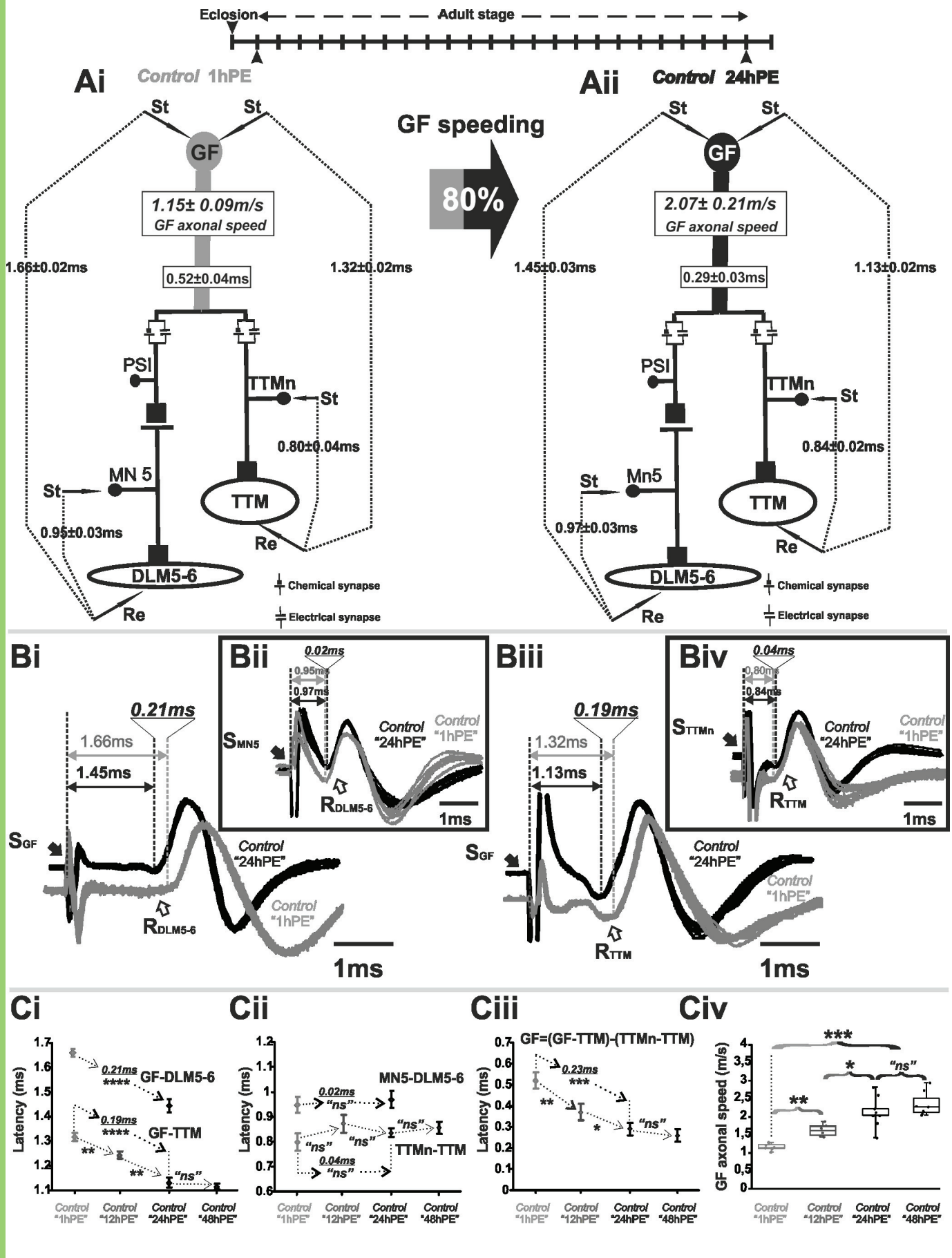

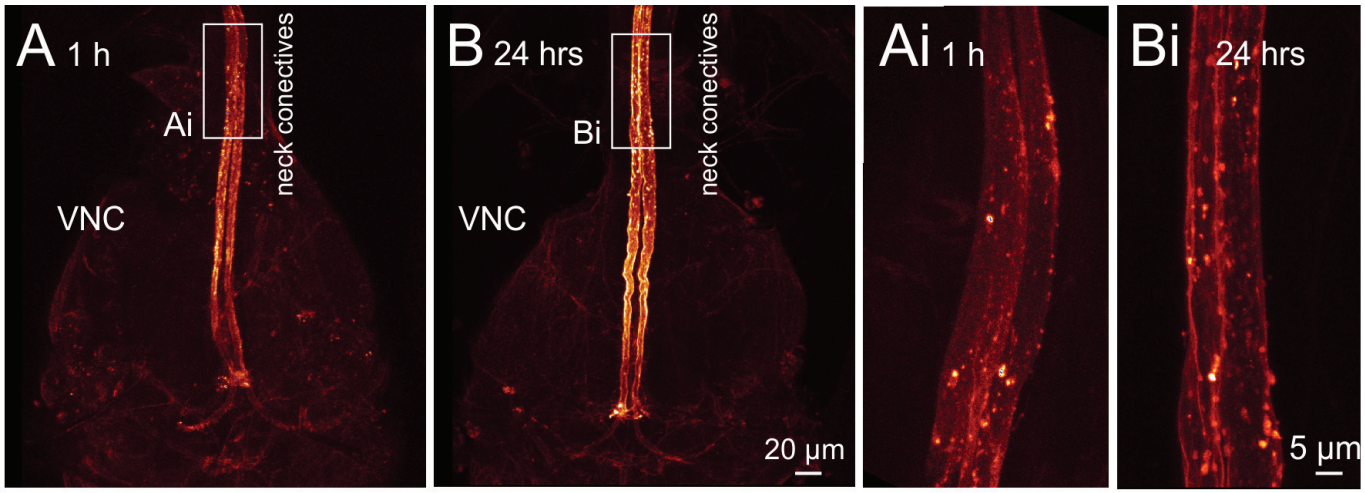

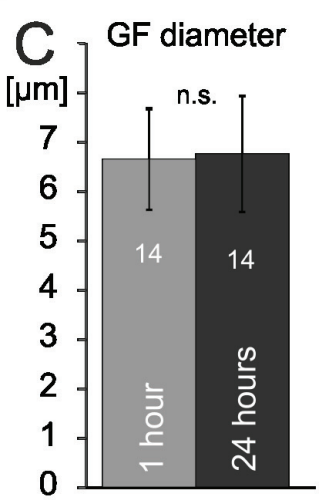

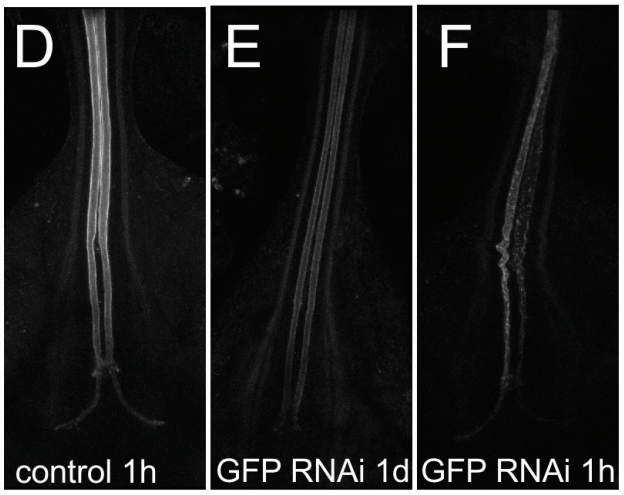

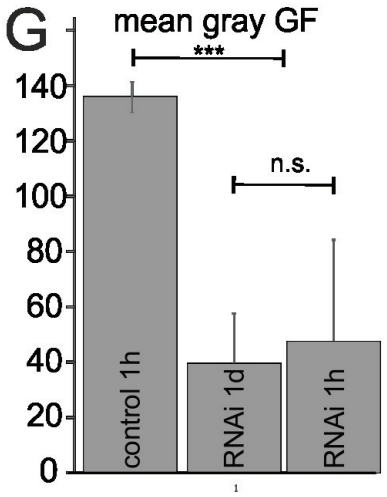

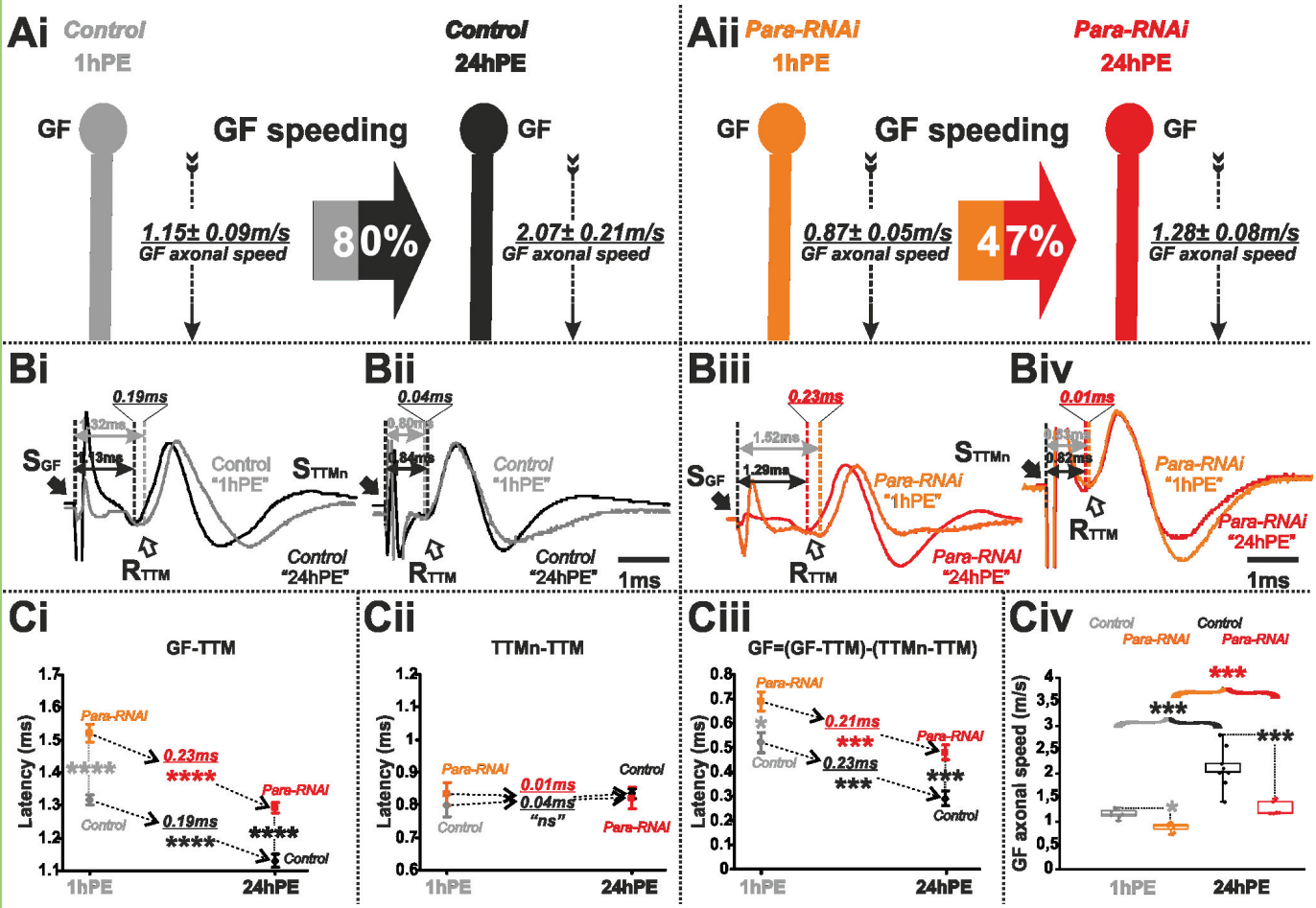

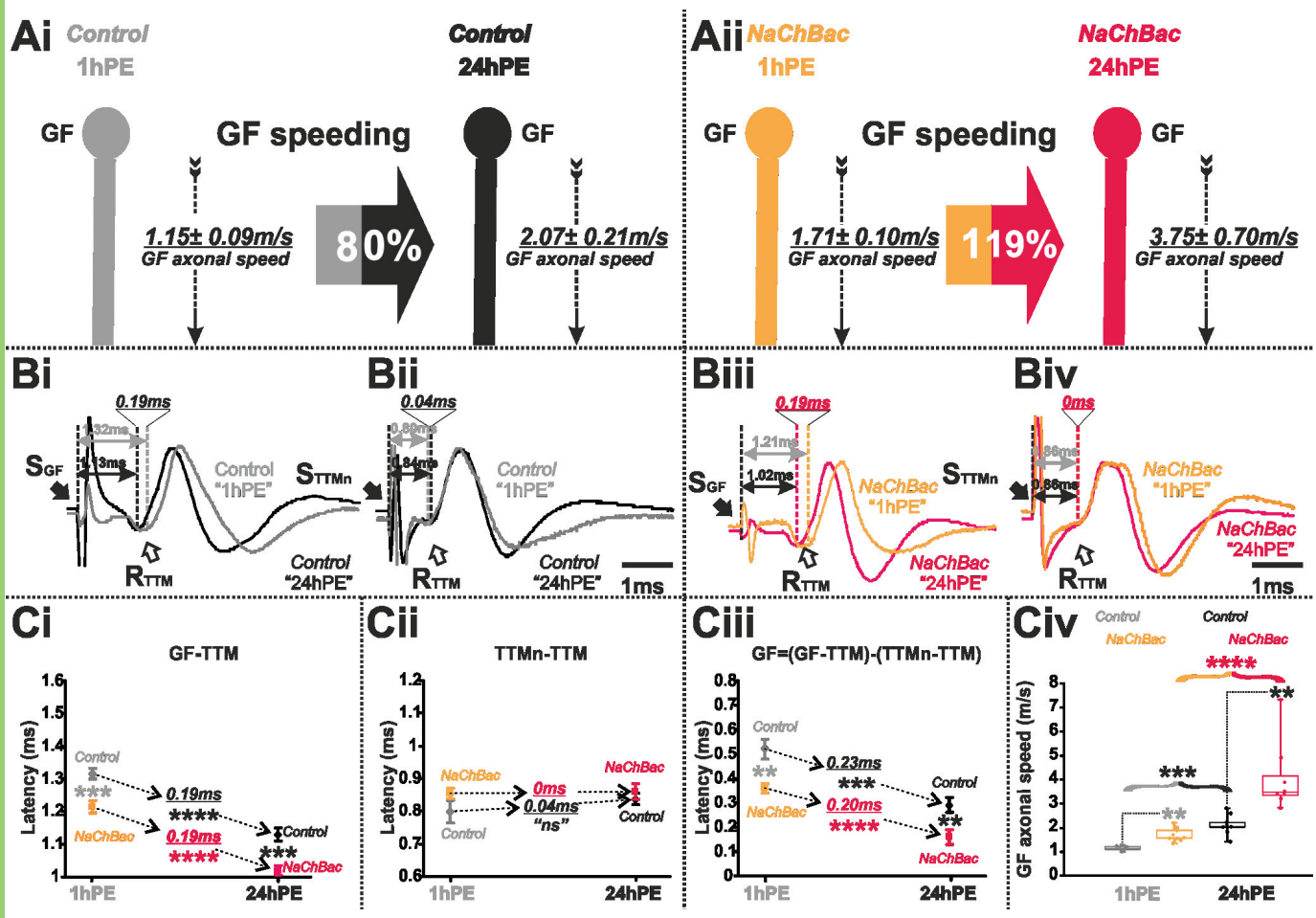

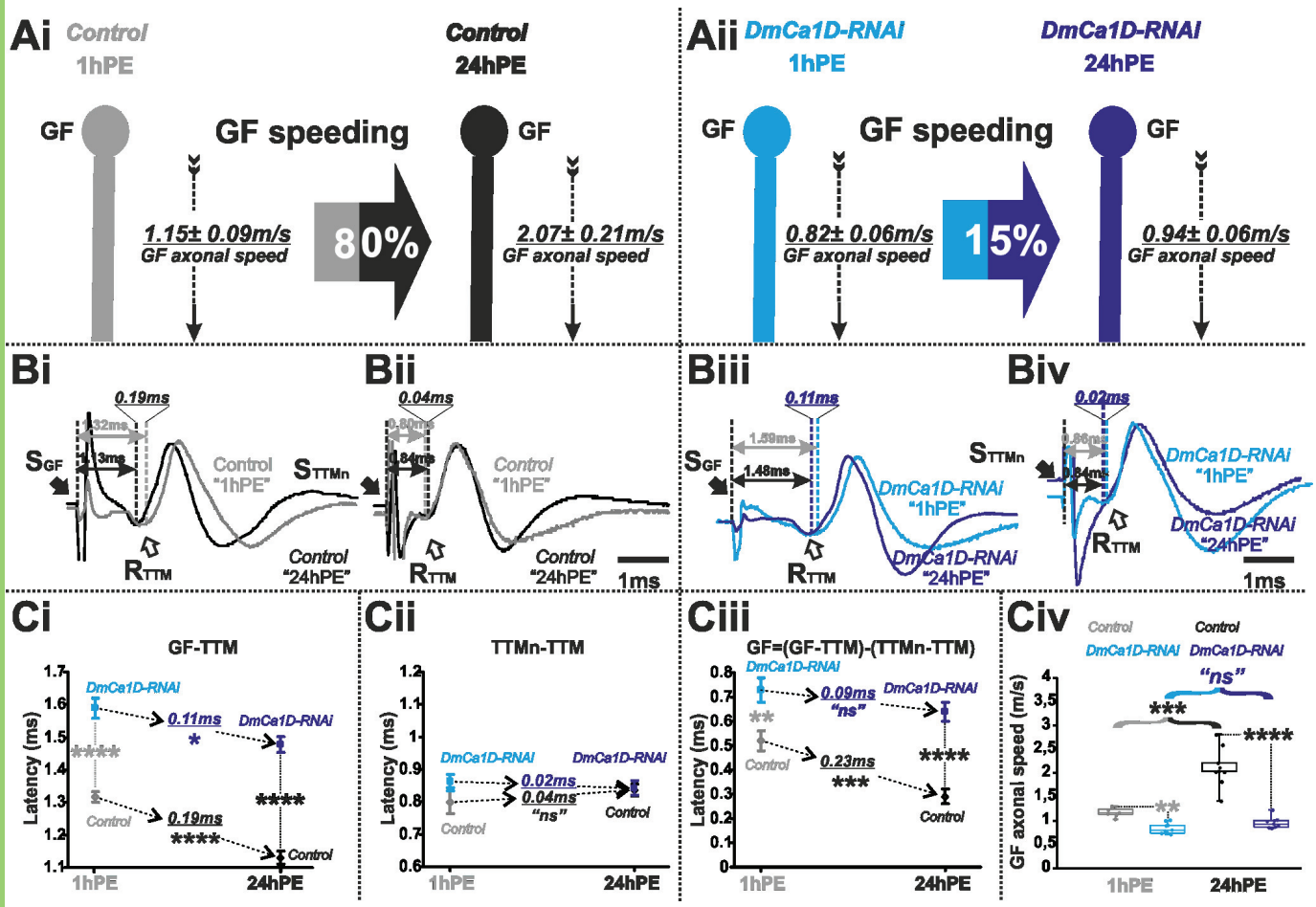

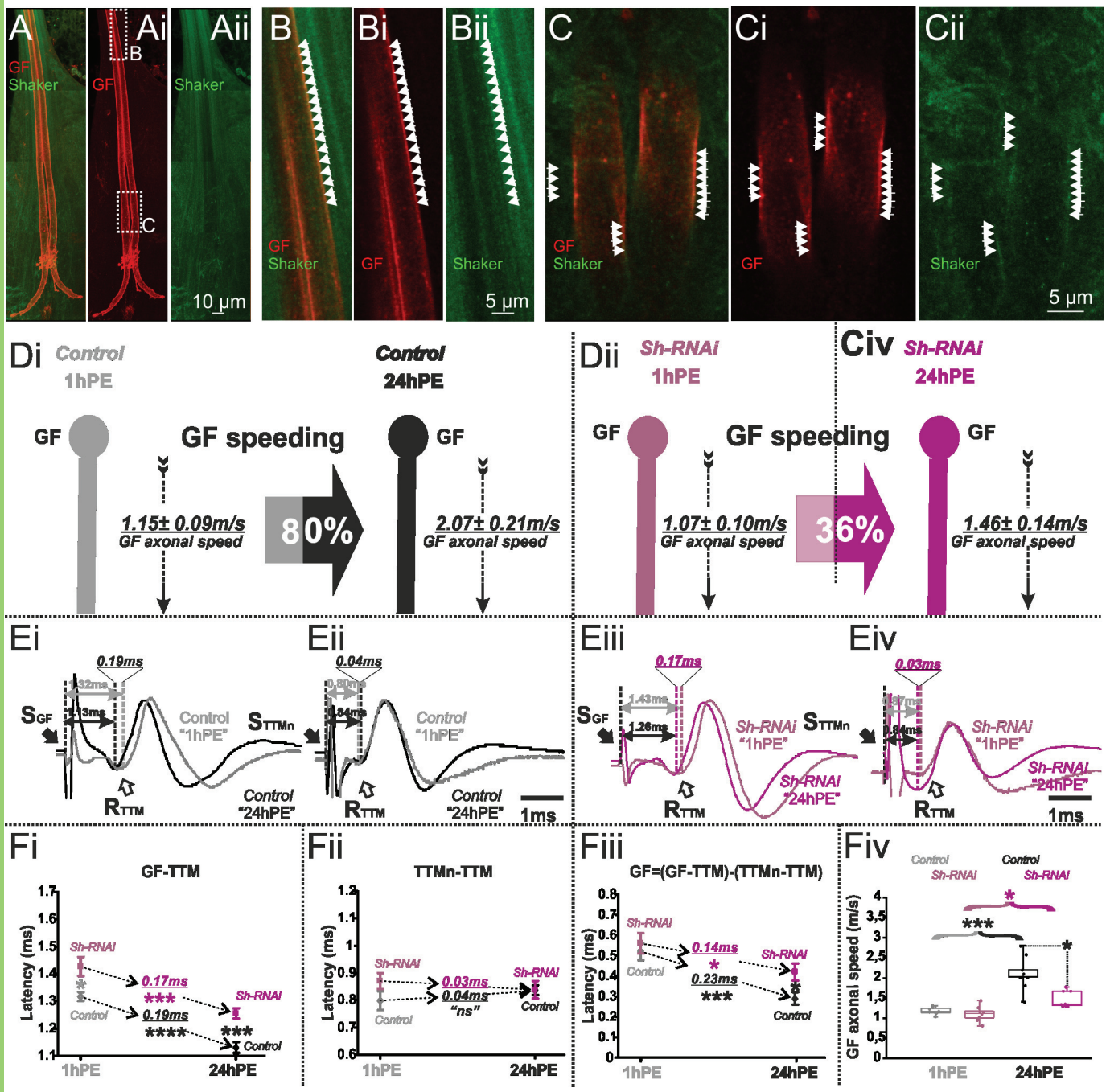

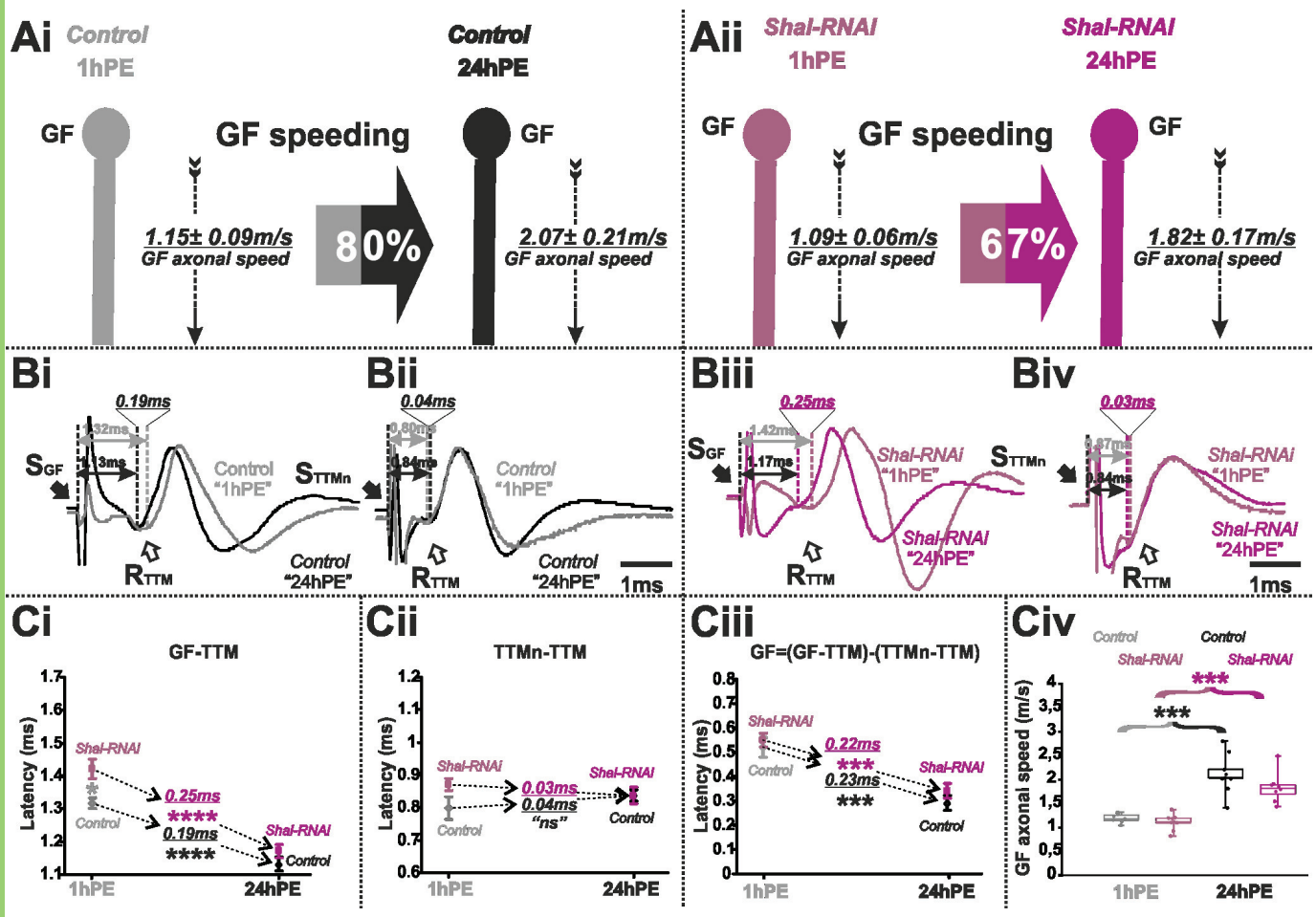

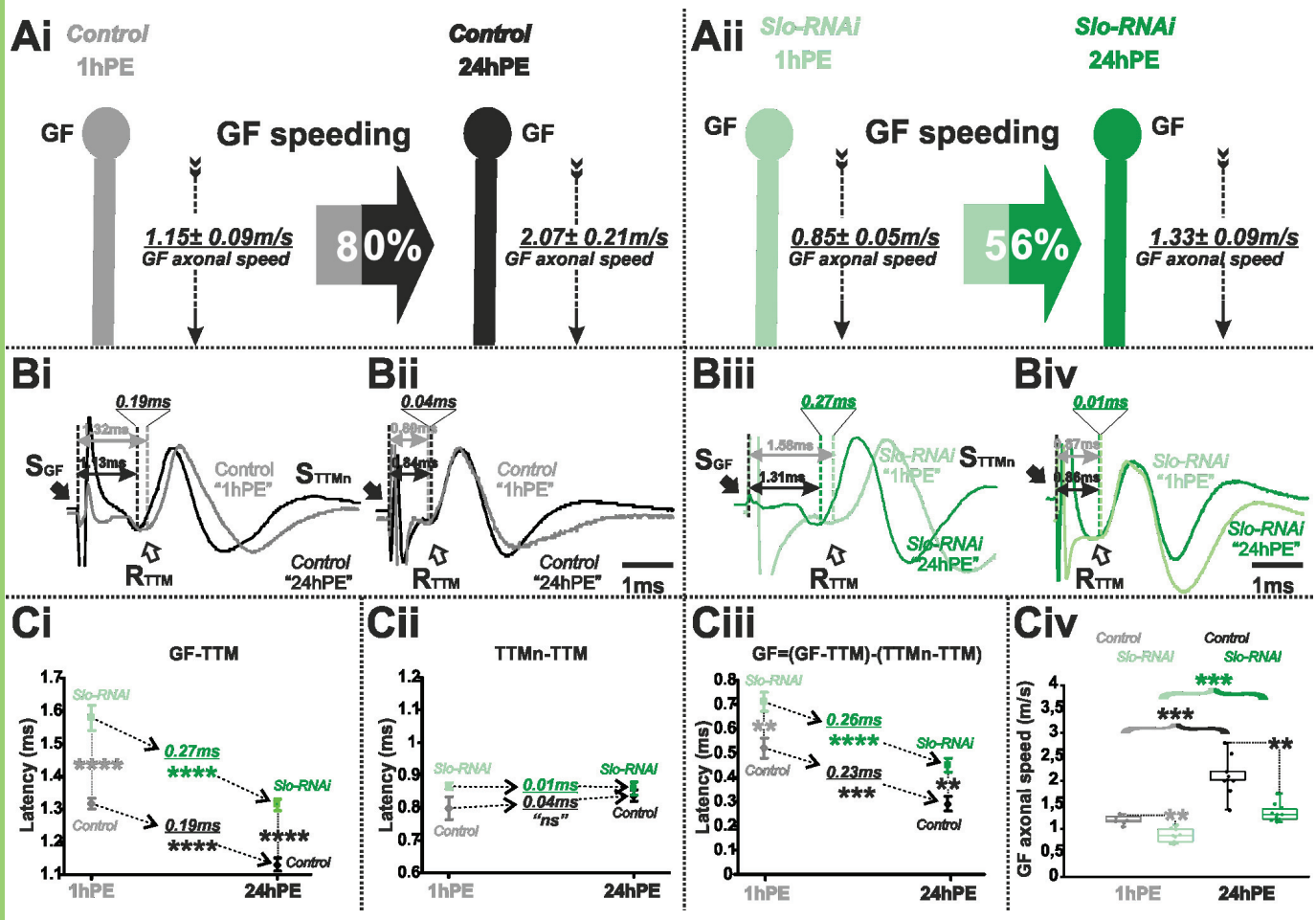

Table1. Latency measurements

	GF-TTM Mean±SEM (n)		TTMn-TTM Mean±SEM (n)		GF=(GF-TTM)-(TTMn-TTM) Mean±SEM (n)	
Genotype	1hPE	24hPE	1hPE	24hPE	1hPE	24hPE
Control	1.32±0,02ms (7)	1.13±0,02ms (9)	0.80±0,04ms (5)	0.84±0,02ms (8)	0.52±0,04ms (7)	0.29±0,03ms (9)
Para-RNAi	1.52±0,03ms (8)	1.29±0,03ms (8)	0.83±0,03ms (5)	0.82±0,03ms (5)	0.69±0,04ms (8)	0.47±0,03ms (8)
NaChBac	1.21±0,02ms (9)	1.02±0,01ms (8)	0.86±0,02ms (6)	0.86±0,02ms (7)	0.35±0,02ms (9)	0.16±0,03ms (8)
DmCa1D-RNAi	1.59±0,03ms (9)	1.48±0,02ms (9)	0.86±0,02ms (5)	0.84±0,02ms (6)	0.73±0,05ms (9)	0.64±0,04ms (9)
Sh-RNAi	1.43±0,04ms (8)	1.25±0,02ms (8)	0.87±0,03ms (5)	0.84±0,03ms (5)	0.56±0,05ms (8)	0.41±0,04ms (8)
Shal-RNAi	1.42±0,03ms (9)	1.17±0,02ms (8)	0.87±0,02ms (6)	0.84±0,03ms (7)	0.55±0,03ms (9)	0.33±0,03ms (8)
Slo-RNAi	1.58±0,04ms (9)	1.31±0,02ms (10)	0.87±0,01ms (5)	0.86±0,02ms (7)	0.71±0,04ms (9)	0.45±0,03ms (10)

Table2. % change in GF axonal conduction speed

	% change due to "knockdown" or "expression" of genes encoding ionic channels		% change due to postnatal maturation
Genotype	1hPE	24hPE	1-24hPE
Control	-------	------	80% ***
Para-RNAi	-32% *	-62% ***	47% ***
NaChBac	+49% ***	+81% **	119% ****
DmCa1D-RNAi	-40% **	-120% ****	15% "ns"
Sh-RNAi	-7% "ns"	-42% *	36% ***
Shal-RNAi	-6% "ns"	-14% "ns"	67% ***
Slo-RNAi	-35% **	-56% **	56% ****